Study of Polymers for Membrane and for Flocculation/Dewatering of Mature Fine Tailings

by

Dan Zhang

A thesis submitted in partial fulfillment of the requirements for the degree of

Master of Science
in
Chemical Engineering

Department of Chemical and Materials Engineering
University of Alberta

© Dan Zhang, 2016

Abstract

This thesis is composed of two parts. The first part deals with the fabrication of antifouling membranes based on polyethersulfone (PES) and cellulose nanocrystals (CNC). PES/CNC nanocomposite membranes were prepared by non-solvent phase-inversion method. The effects of PES/CNC composition on membrane properties and performance were investigated. The contact angle and water content results revealed that the hydrophilicity of the membranes enhanced significantly by increasing the CNC content in the casting solution. The pure water flux was improved with an increase of CNC concentration up to 1.0 wt. %, and decreased with further addition of CNC in the casting solution up to 5.0 wt.%. Bovine serum albumin (BSA) rejection was also improved by increasing CNC content due to the formation of smaller pore size and thicker skin layer of the nanocomposite membranes. The antifouling property was significantly improved after blending CNC as quantified by measuring the flux recovery ratio, which can be attributed to the improved hydrophilicity.

The second part of the thesis deals with the preparation of new temperature-responsive and cationic polymers for flocculation and dewatering of mature fine tailings (MFT). In this section, *N*-isopropylacrylamide (NIPAM) homopolymer and statistical copolymer of NIPAM and 2-aminoethyl methacrylamide hydrochloride, poly(AEMA-*st*-NIPAM), were synthesized by conventional free-radical polymerization for flocculation and dewatering of MFT. A mixture of polyNIPAM and cationic poly(AAm-*st*-DADMAC) was studied and the effects of mixture ratio, temperature and polymer dosage on MFT settling rate, supernatant turbidity, solid content and

water recovery were evaluated to determine the flocculation performance. Temperature-responsive polyNIPAM can achieve high initial settling rates (ISR) and water recovery. However, the addition of only polyNIPAM cannot achieve high clarity of supernatant. The addition of both cationic poly(AAm-*st*-DADMAC) and polyNIPAM can improve significantly the clarity of supernatant. Enhanced solid content can be achieved by polyNIPAM when temperature decreased from 50 to 25 °C. Copolymer poly(AEMA-*st*-NIPAM) can improve both ISR and clarity of supernatant, while the secondary enhanced solid content is lower due to the strong electrostatic force between particles and AEMA, which is not affected by temperature. Dosing an optimum mixture ratio of polyNIPAM and poly(AAm-*st*-DADMAC) can improve ISR, clarity of supernatant, water recovery and solid content.

Preface

Chapter 3 of this thesis will be submitted for publication as Zhang, D.; Karkooti, A.; Sadrzadeh, M.; Thundat, T.; Narain, R. “Fabrication of antifouling polyethersulfone (PES)/cellulose nanocrystals (CNC) nanocomposite membranes.”

Chapter 4 of this thesis will be submitted for publication as Zhang, D.; Thundat, T.; Narain, R. “Flocculation and Dewatering of Mature Fine Tailings Using Temperature-Responsive Cationic Polymers.”

Dedication

I dedicate this work to my family and friends

who support me in every endeavor I seek.

Acknowledgement

I would like to give my sincere gratitude to my supervisors, Dr. Ravin Narain and Dr. Thomas Thundat for their kind guidance, encouragement, and support for my master degree study. Dr. Narain and Dr. Thundat are professors with rich knowledge and experience in chemical engineering field. Under their guidance, I obtained both theoretical knowledge and practical experience.

I would also like to express my gratitude to Dr. Mohtada Sadrzadeh. He gave me a lot guidance for experimental design and provided me experiment equipments for the membrane project. His PhD student Amin Karkooti also provided me a lot of help for the membrane project. I would like to appreciate their patience to help me to revise my manuscript and provide insightful comments.

I am also thankful for all colleagues in our lab, including Masanori Nagao, Christopher Afacan, Lu Han, Pratyawadee Singhsa, Diana Diaz and Yi-Yang (Kevin) Peng.

List of Contents

List of Figures

List of Tables

List of Abbreviations

AEMA	2-aminoethyl methacrylamide hydrochloride
APS	Ammonium persulfate
BCA	Bicinchoninic acid assay
BSA	Bovine serum albumin
CA	Cellulose acetate
CNC	Cellulose nanocrystals
GPC	Gel permeation chromatography
ISR	Initial settling rate
LCST	Lower critical solution temperature
MFT	Mature fine tailings
MWCO	Molecular weight cutoff
NF	Nanofiltration
NMR	Nuclear magnetic resonanc
NTU	Nephelometric turbidity units
PA	Polyamide
PAN	Polyacrylonitrile
PE	Polyethylene
PEG	Polyethylene glycol
PEI	Polyetherimide
PES	Polyether sulfone
PET	Polyethylene terephthalate

Poly(AAm-co-DADMAC)	Poly(acrylamide-co-diallyldimethylammonium chloride)
PolyNIPAM	Poly (*N*-isopropylacrylamide)
PS	Polysulfone
PTFE	Polytetrafluoroethylene
RO	Reverse osmosis
TDS	Total dissolved solids
TEMED	*N,N,N′, N′*-tetra- methylenediamine
TGA	Thermogravimetric analysis
TOC	Total organic carbon
UF	Ultrafiltration

Chapter 1 Introduction

1.1 Water shortage problem and water treatment techniques

The world witnessed rapid development and population explosion in last century and such rapid growth resulted in great pressure on water resources. Water is required by all human activities from daily life to industry. Therefore ensuring sufficient water supply is important for human well-being. Although 71% of earth area is covered by ocean, the warning of water shortage in the world is common. As shown in Figure 1.1, water shortage increased extremely rapid from 1960. The world population living under water shortage increased from 9% (280 million people) in 1960 to 35% (2300 million) in 2005 [1].

Therefore, water management techniques are required in order to improve water recovery rates and water qualities. In oil sands industry, one barrel bitumen extracted by water-based method needs 2-3 m^3 water, so the amount of water required by oil extraction industry is massive. Water recovered from oil sands tailings can be reused into oil extraction process, so proper tailing management can accelerate the solid-liquid separation process and improve water recovery rates and clarity to meet the needs of oil extraction process. Effective tailing management can also reduce the volume of tailings, thus less area is needed for the tailing ponds. Typical tailing management including nature process, biological treatment, physical/mechanical process, and chemical treatment. All of these treatment are aiming to improve the flocculation and dewatering, so that the solid-liquid separation can occur in shorter time. High water recovery can improve water recycle efficiency, meaning less fresh water is needed and can save more water.

Another water treatment technique is polymer membrane based process for water purification. The membrane can be described as a barrier that allows the components smaller than membrane pore

size to permeate while the components larger than pore size are retained and separated from the solute. Pressure needs to be applied at the feeding solution side, and the pressure difference between two sides is the driving force for the solution.

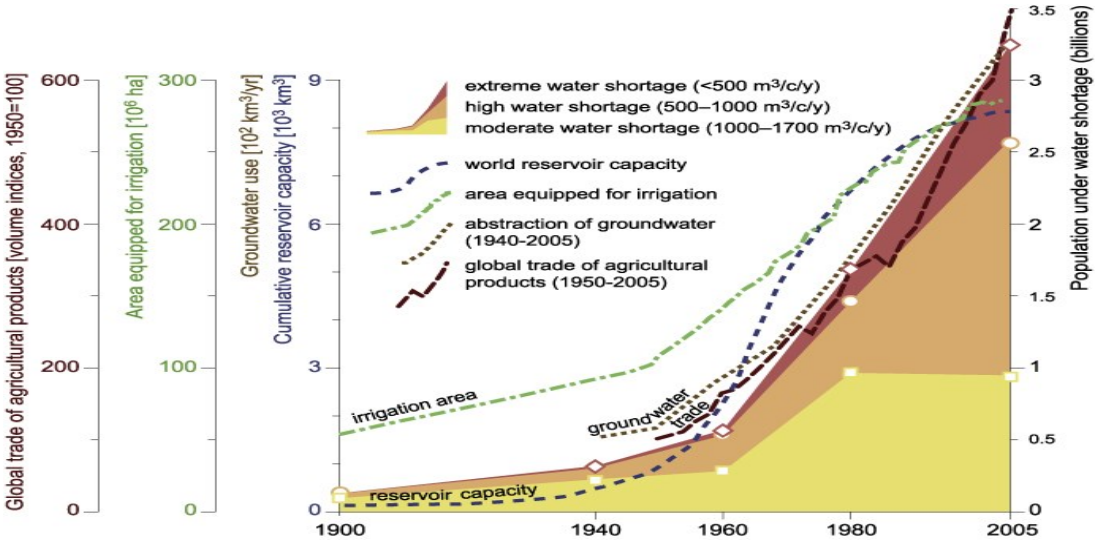

Figure 1.1. Comparison of population under water shortage [1]

1.2 Water recovery from oil sands tailings

1.2.1 Composition of oil sands tailings

In oil sands industry, large amount of tailings are produced after oil extraction, which contain water, coarse sands, clay, and residual bitumen. These tailings are discharged into tailing ponds for solid-liquid separation. In the tailing ponds, tailings are separated into three layers: the heaviest coarse sands settle to the bottom and water released from tailings form the top layer, which can be recycled into oil extraction process. The middle layer, which contains fine clays, water and residual bitumen, is known as mature fine tailings (MFT). MFT forms “gel-like” suspensions with particles which size is smaller than 44 μm [2]. Due to the small size of particle and high water retention capacity [3], MFT suspensions take long period to settle and release the entrapped water. The MFT

formation mechanism occurs in tailing ponds is exhibited in Figure 1.2.

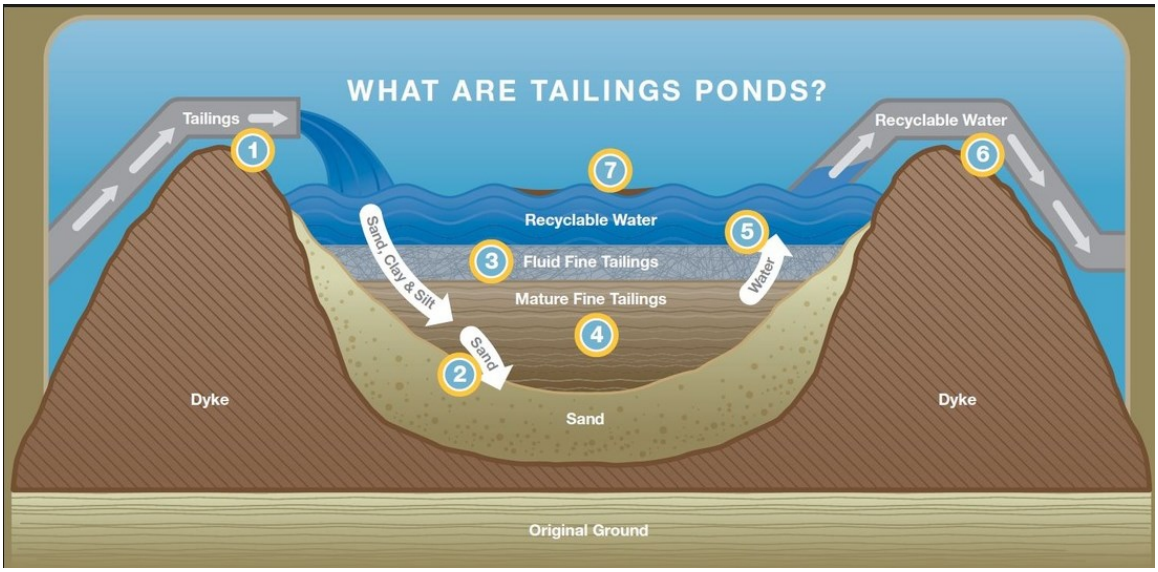

Figure 1.2.The formation mechanism of mature fine tailings (MFT) [4].

1.2.2 Review of tailings managements

In order to accelerate the settling rates of MFT and enhance the water recovery rates, a large amount of works has been conducted by many researchers. There are some techniques such as natural process, biological treatment, physical/mechanical process, and chemical treatment.

1.2.2.1 Natural process

The most traditional one is freeze-thaw technology. Tailings are frozen in winter and then thawed in the next summer. The MFT form a “solid-like” cake with fissured structure during the freeze step in winter, and this structure can drain quickly when MFT is thawed in the next summer, so the solid-liquid separation can be accelerated and water drained in summer can be reused in oil extraction process. It has been reported that the solids content of MFT increased from 30% to around 45% after freeze-thaw treatment [5]. Although freeze-thaw method is simple and the cost is lower, the drawbacks of this method are labor intensive and time consuming. In addition, large

area is needed and managing the pumping of fluids during extremely cold temperatures is challenging.

1.2.2.2 Biological treatment

Suitable species are planted on the high water content tailings, and the dewatering is achieved by transpiration through the leaves and root system [6]. Large amount of water can be transferred during the plant growing season. The mechanism of plant (evapotranspiration) dewatering process is shown in Figure 1.3. The root development increases bearing capacity at the tailings surface, reducing the requirement of pressure equipment for the reclamation and improve the energy efficiency. However, there are many limitations of this method. First, the high saline tailings limit the species that can be applied, and introducing non-native species may cause the problem of species invasive. Second, the depth of dewatering achieved by room is very limited. Third, this method is also depended on local weather and climate conditions.

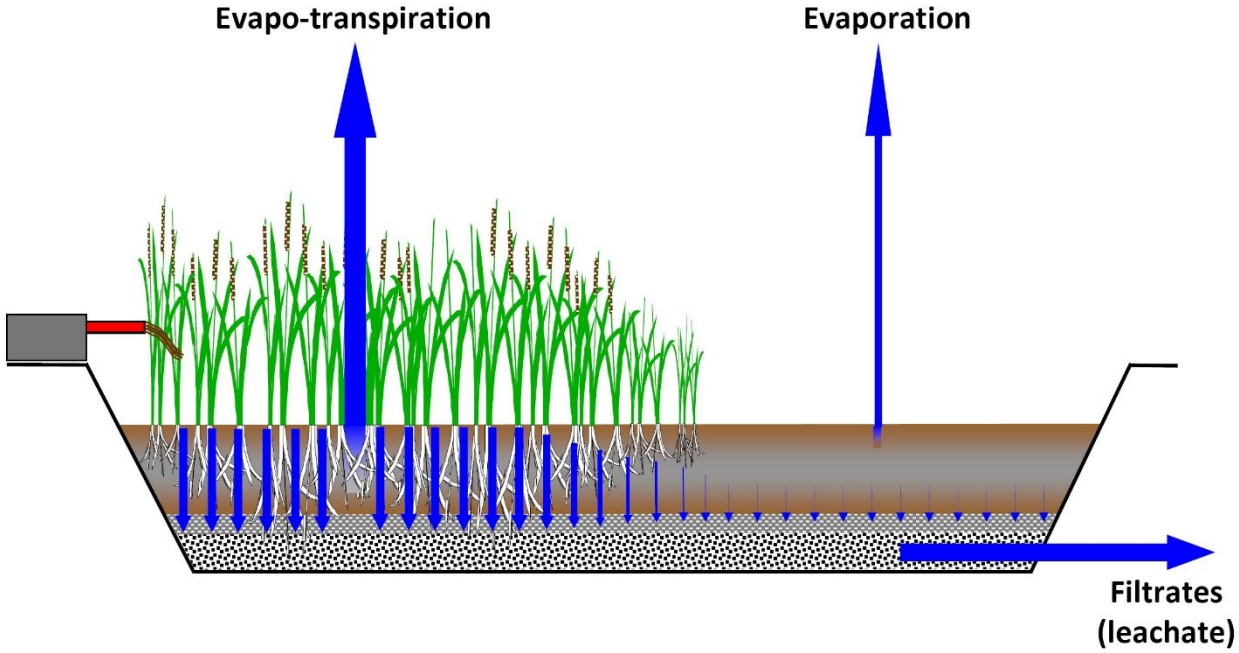

Figure 1.3.The mechanism of plant (evapotranspiration) dewatering process [7].

1.2.2.3 Physical/mechanical processes

The physical/mechanical processes including filtration[8], centrifuge [9], and electrical treatment [10-12]. The most traditional one is filtration, which has low environmental impacts while the cost is relatively high. Centrifuge is another common method, and it has been reported that this method can produce tailings with around 60% solid contents. Centrifuge requires relatively small storage area and can recover large amount of water, but the cost is high and requires experienced operators. The third one is electrical treatment. The working principle of electrical treatment is applying direct current (DC) electric field to the negatively charged particles, thus the particles will move to the positive (anode) electrode, leading to higher settling rate.

1.2.2.4 Chemical treatment

Chemical treatment, such as coagulants and flocculants. In particular, chemical treatment has gathered attention because it is high efficiency. Coagulants like gypsum can introduce calcium cations to neutralize negative charged particles and reduce the repulsion between particles. Synthetic polymers are also useful for effective flocculation, and it is one of the most widely used methods to dose polymer flocculants into MFT suspension to bridge the fine particles and subsequently flocculate these particles into big flocs. Researchers have synthesised inorganic/organic hybrid polymeric flocculants such as $Al(OH)_3$-polyacrylamide (Al-PAM) to accelerate the settling rate and enhance dewatering. The cationic nature of imbedded aluminum hydroxide can improve the performance of polyacrylamide (PAM) [13-16]. Recently, temperature stimulus response polymer poly(*N*-isopropylacrylamide) (PolyNIPAM) has been reported as novel flocculant to accelerate settling rate and enhance consolidation [17-22]. PolyNIPAM contains acrylamide and isopropyl groups, and when temperature is below its lower critical solution temperature (LCST), which is around 32 °C, acrylamide groups are hydrate and the polymer chain

is stretched and water soluble, whereas when temperature is above LCST, isopropyl group dehydrate and the polymer conformation change to coil-like structure and become hydrophobic [22]. PolyNIPAM can adsorb onto particle surface at temperature below LCST by hydrogen bonds. Then the polymers experience phase transition and get hydrophobic by increasing the temperature above LCST, resulting in collapse of polymer chains. As a consequence, particles in tailings suspension are rapidly flocculated and settled due to the strong hydrophobic interactions. Li et al. [17] studied the adhesion force between kaolin particles and polyNIPAM by AFM. The results showed that the adhesion force increased from almost zero to 3.5 mN/m by increasing temperature from room temperature to 40 °C, and the repulsion between particles decreased to almost zero after increasing temperature. After forming big flocs, the sediment was cooled blow LCST so the polymer become hydrophilic again and detach from particles, thus small particles can fill the gap between flocs to further enhance consolidation [23-25]. However, the nonionic property of polyNIPAM limits its application due to failure to neutralize some charged particles [19, 26]. To further improve the performance of polyNIPAM, many researchers have introduced cationic groups to polyNIPAM in order to achieve higher flocculation ability [27]. Lu et al. [18] has synthesised polyNIPAM based copolymer poly($AEMA_{51}$-*st*-$MAAmBo_{76}$-*st*-$NIPAM_{381}$) containing 2-aminoethyl methacrylamide hydrochloride (AEMA) and 5-methacrylamido-1,2-benzoboroxole (MAAmBo) to increase the settling rate and water clarity of clay suspension. The copolymer showed higher settling rate because of the electrostatic interaction between cationic AEMA and negatively charged particles. The copolymer can work as polyelectrolyte to adsorb onto charged particle surface by electrostatic force, resulting in higher clarity of recovered water.

1.3 Review of membrane based water treatment

1.3.1 Microfiltration

Microfiltration (MF) is a physical process to remove suspended solid particles in the solution. The MF membrane can remove particles larger than pore size, which is around 0.1 to 10 μm. The separation mechanism is based on sieving. MF is usually used as a pre-treatment process for other treatments such as ultrafiltration and reverse osmosis, and sometimes coagulants are required [28]. The microfiltration membranes are made from polymers such as cellulose acetate (CA), polytetrafluoroethylene (PTFE), polysulfone (PS), polyether sulfone (PES) and polyethylene terephthalate (PET) [29].

1.3.2 Ultrafiltration

Ultrafiltration (UF) process is similar to MF. The separation mechanism of both is sieving. While UF membranes have smaller pore size at range 0.001 to 0.02 μm, so UF can remove smaller particles compared to MF[30]. UF can be served as pre-treatment for nanofiltration and reverse osmosis. Most operation mode of UF is dead-end system, in which the feeding solution flow facing through the membrane, and the larger molecular solutes are accumulated on the membrane surface and decreases the flux, resulting in fouling problem. Therefore membrane cleaning becomes necessary after a period of operation. The UF membranes are also made from polymers such as polytetrafluoroethylene (PTFE), polyethylene terephthalate (PET), polyvinylidene fluoride (PVDF), polypropylene (PP), polyethylene (PE), polysulfone (PS), and polyethersulfone (PES), and can be used in manufacturing, food and beverage processing [31].

1.3.3 Nanofiltration

Nanofiltration (NF) membranes have higher selectivity than MF and UF membranes and can achieve molecular weight cutoff (MWCO) at 200 Daltons. NF membranes are also more energy

efficiency and require lower operation pressure. The separation mechanisms of NF membranes are diffusion and exclusion. The NF membranes can be used to remove total organic carbon (TOC), salinity, total dissolved solids (TDS) and multivalent ions from surface water and fresh groundwater and soften the treated water. The operation system of NF membrane can be cross-flow, which causes less fouling problems (Figure 1.4). However, the costs of NF manufacture and maintenance are high, which is the main drawback of NF membranes. The NF membranes can be made from polymers such as polyamide (PA), polyethersulfone (PES), polyetherimide (PEI) and polyacrylonitrile (PAN) [30].

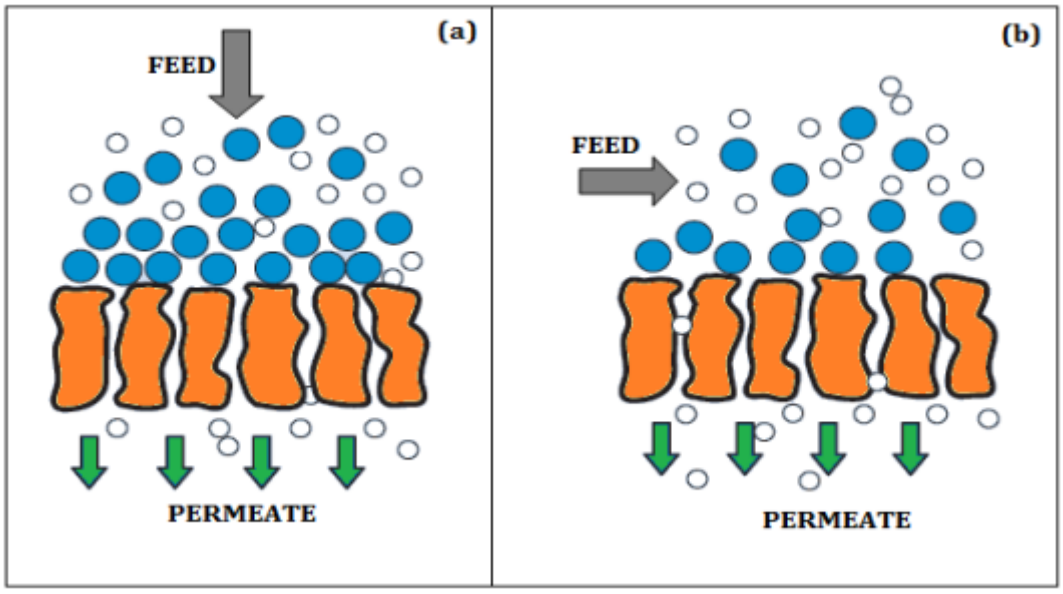

Figure 1.4. (a) dead-end filtration system (b) cross-flow filtration system [30].

1.3.4 Reverse Osmosis

Reverse osmosis has highest selectivity among MF, UF and NF. Reverse osmosis can remove ions, molecules, and larger particles from drinking water. Water is the only component that can pass through the semipermeable membrane. External pressure needs to be applied to overcome the osmosis pressure. The reverse osmosis process is shown in Figure 1.5. The membranes can be

made from polymers such as cellulose acetate (CA), polyamide (PA) and polyacrylonitrile (PAN). The reverse osmosis technique can be applied for water purification and concentrating of juice and cheese [30]. The selectivity of four different filtration membranes (MF, UF, NF and RO) is shown in Figure 1.6.

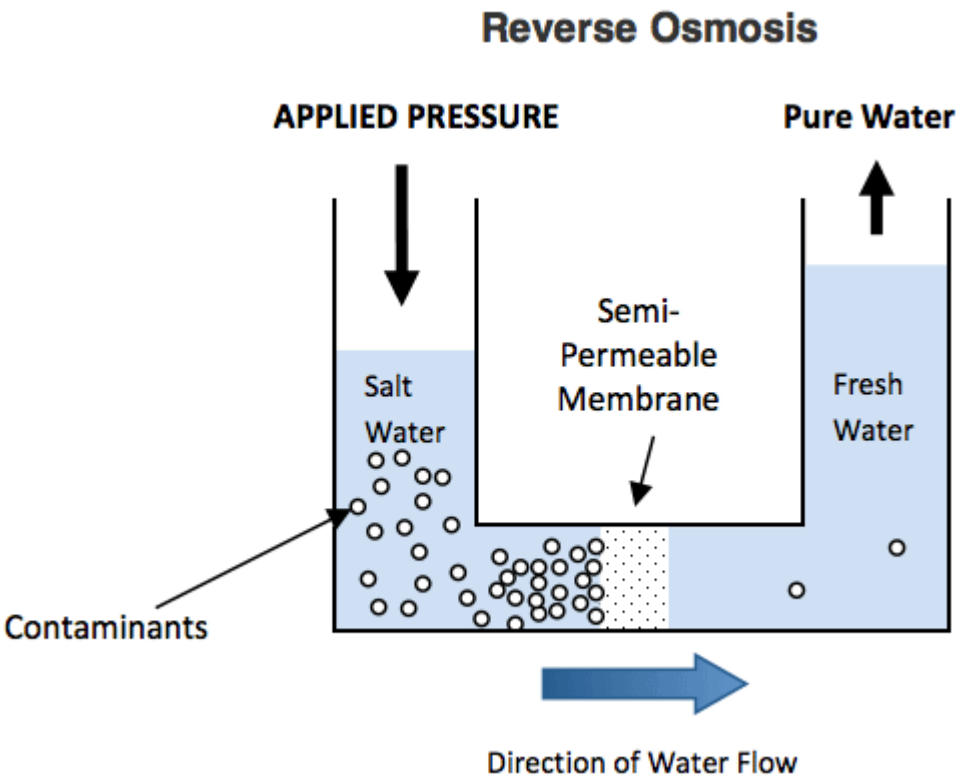

Figure 1.5. Diagram of reverse osmosis process [32]

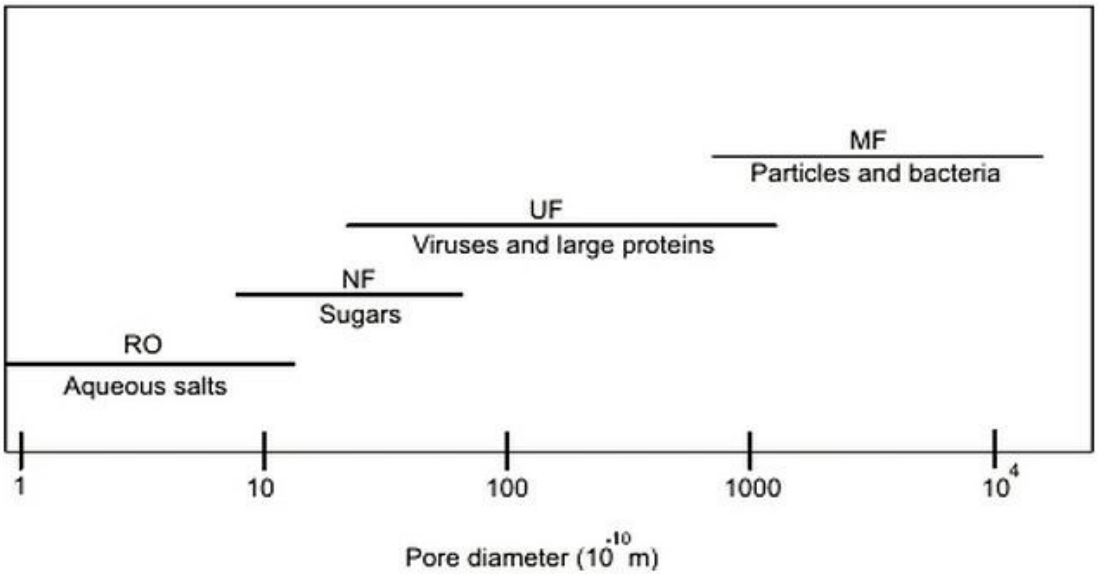

Figure 1.6. Selectivity comparison of Microfiltration (NF), Ultrafiltration (UF), Nanofiltration (MF) and Reverse Osmosis (RO)[33].

Chapter 2 Experimental techniques

2.1 Gel permeation chromatography (GPC)

Gel permeation chromatography (GPC) is a type of size exclusion chromatography. The development of gel permeation chromatography can be backed to 1960, Vaughan et al. [34] used the insoluble cross-linked polystyrene as medium to separate polymers with different molecular weight. A typical GPC was shown in Figure 2.1 and the basic elements including a pump injector, column, detector, and the data processing equipment. The pump is responsible for delivery the polymer in solution through the system, and the pump must deliver the polymer components with different viscosity at the same flow rates. The injector can introduce polymer solution into the mobile phase. The separation of components take place in the column set, and detected by differential refractometer (RI).

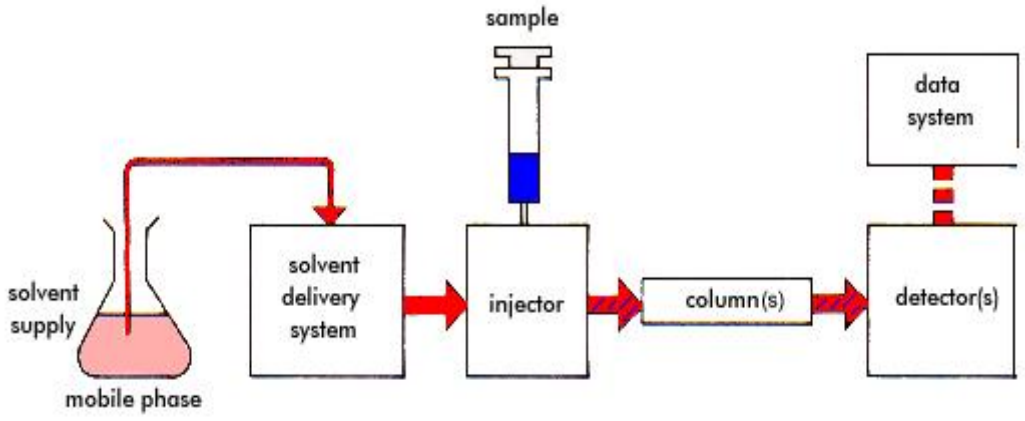

Figure 2.1. The schematic drawing of gel permeation chromatography (GPC) [35].

GPC separates based on the size of the analytes (Figure 2.2). The smaller analytes have higher possibility to enter the pores of media in the column and therefore spend longer time to pass through the column, resulting in longer retention time. On the other hand, it is harder for the larger

analytes to enter the pores, so they spend less time to pass through and eluted faster than the smaller analytes. The molecular weights separation ability varies depends on different columns.

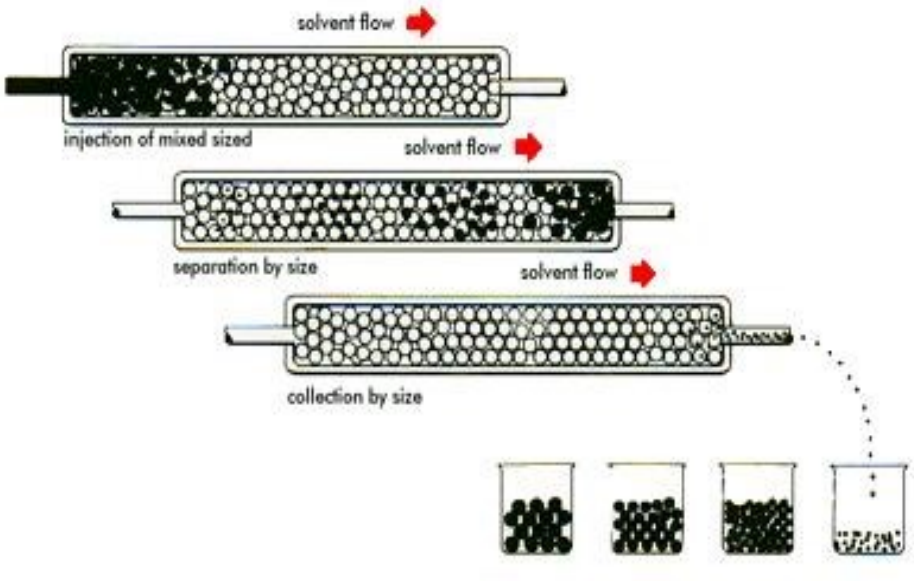

Figure 2.2. The seperation priciple of gel permeation chromatography (GPC) [35].

2.2 Phase inversion technique

Phase inversion is a widely used technique for membranes fabrication. The scheme of membrane preparation by phase inversion process is shown in Figure 2.3. During the phase inversion process, the polymer solvent is removed, leaving a porous and solid membrane. Phase inversion is a demixing process during which a homogenous polymer solution transfers from liquid to solid state [36]. When solution immersed into coagulation bath containing non-solvent, the solvent diffuse into non-solvent bath while the non-solvent penetrate the casted polymer solution (Figure 2.4). The exchange of solvent and non-solvent induce the demixing. So the solvent and non-solvent must be miscible [37]. The flow rate of non-solvent (J_1) and solvent (J_2) decide the types of membranes obtained. When $J_2>J_1$, the ultrafiltration membranes are formed [36]. The exchange

rate between solvent and non-solvent is affected by several parameters including the diffusion force of non-solvent, solubility parameters and physical condition of phase inversion process [38]. The mechanism of membrane formation has been reported by many researchers. Bokhorst et al. [39] reported the formation mechanism of cellulose acetate membranes, and concluded that the top layer is formed by gelation and the porous sublayer is formed by liquid-liquid phase separation. Broens et al. [40] suggested similar results that the formation of porous sublayer is due to the liquid-liquid phase separation while the formation of pores is the result of nucleation and growth of the diluted polymer phase. When polymer solution immersed into coagulation bath, the solvent moves fast from the casted polymer solution while the movement of non-solvent into the casted polymer solution is relatively slow ($J_2>J_1$), so the concentration of polymer at the film/non-solvent interface increase and cross the gel boundary, resulting in the transition from homogeneous solution (H) to gelation (G). The transition process is shown in Figure 2.5. The formation of gel-layer can further work as a resistance to non-solvent out-diffusion. So the higher non-solvent and lower polymer concentration under the top layer can cause demising process and liquid-liquid phase separation occurred and transferred from H to L (Figure 2.5.). Then the demixing gap reach the critical point (CP), resulting in the nucleation and growth of the diluted polymer phase, so the porous sublayer structure is formed [41].

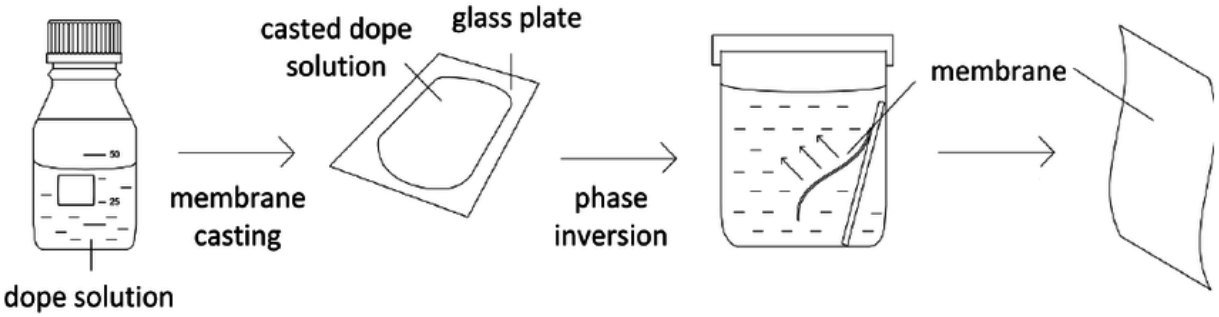

Figure 2.3. Scheme of membrane fabrication via phase inversion [42] .

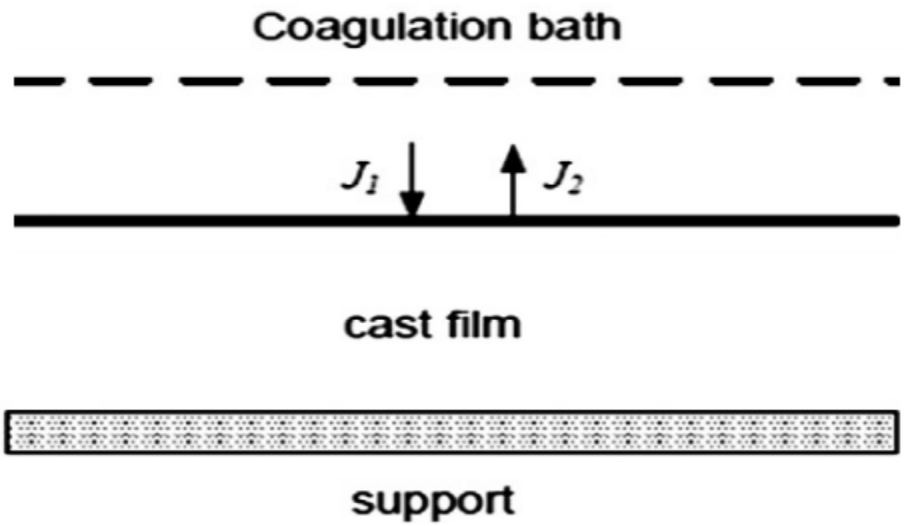

Figure 2.4. Schematic representation of a film/bath interface: J_1 is the non-solvent flux and J_2 the solvent flux [36].

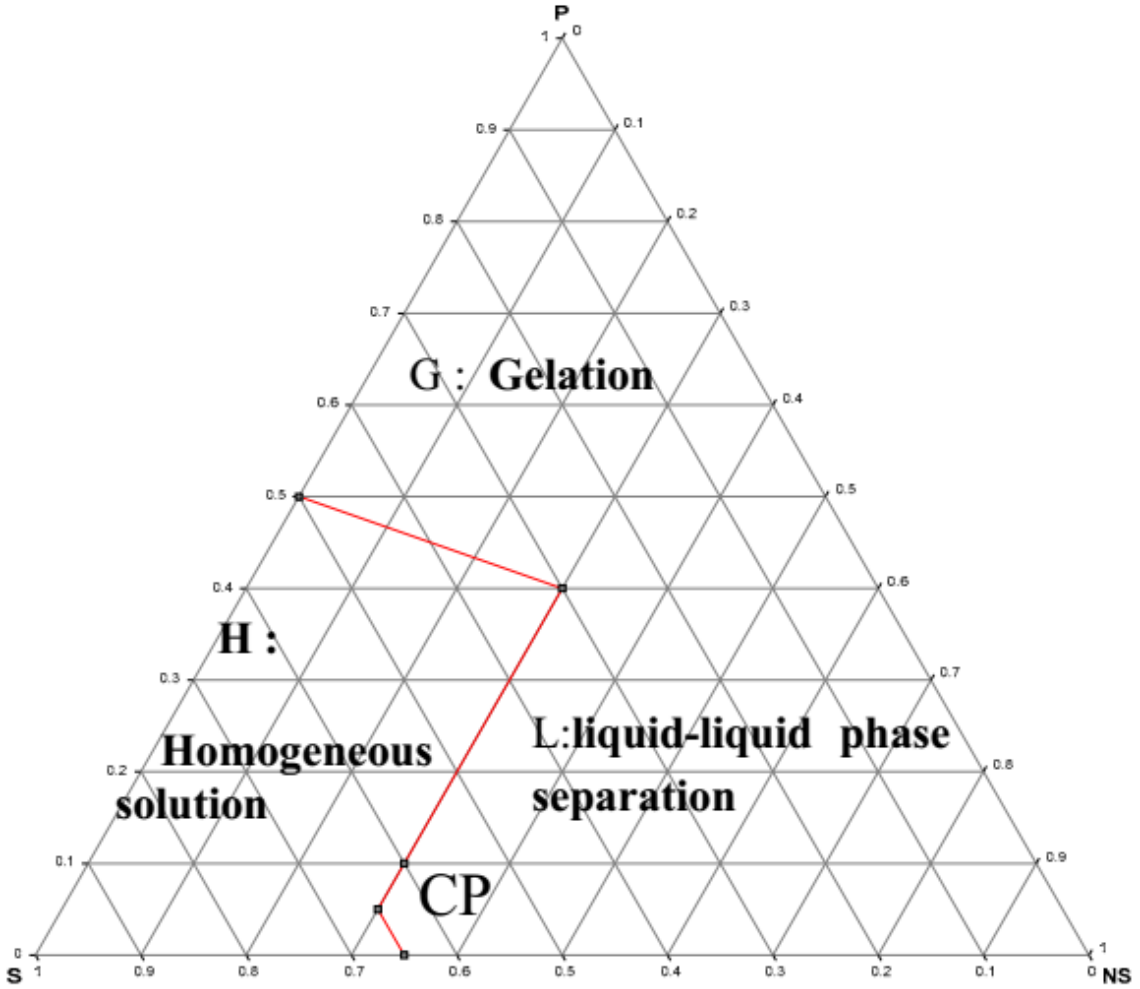

Figure 2.5. Mechanism of formation of asymmetric membrane, ternary phase diagram containing P, polymer; S, solvent; NS, non-solvent; CP, critical point; G, gelation (gel region); L, liquid–liquid phase separation(two phase region); H, homogeneous solution (one phase region) [41]

2.3 Thermogravimetric analysis (TGA)

Thermogravimetric analysis (TGA) is a technique in which the mass of the analytes is measured as a function of increasing temperature. TGA is used to determine the materials stability that exhibit mass loss, which can be caused by the following reasons: chemical reaction, the release of

adsorbed species, and decomposition. All of these indicate that the material is no longer thermally stable [43]. The basic elements of TGA including a balance with a loaded with sample and a furnace which can be programmed for a constant heating rate. The apparatus of TGA is shown in Figure 2.6. TGA can provide information about physical phenomena, such as second-order phase transitions, adsorption and desorption.

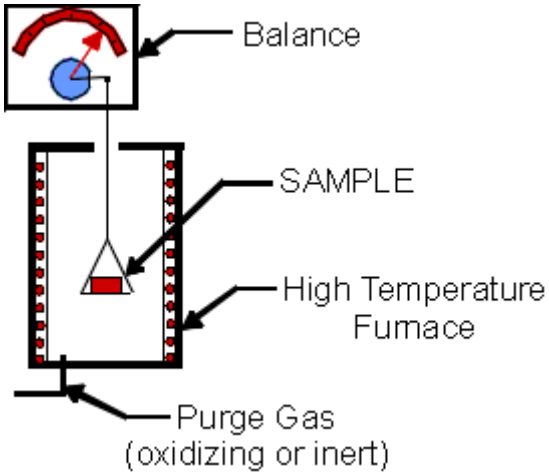

Figure 2.6. A typical TGA system [44].

2.4 BCA Protein Assays

BCA Protein Assay is a formulation based on bicinchoninic acid (BCA) for the colorimetric detection and quantitation of total protein. The configuration of protein, the number of peptide bonds and the presence of four particular amino acids (cysteine, cystine, tryptophan and tyrosine) are reported to be responsible for color formation with BCA [45]. This method is developed based on Biuret reaction, in which protein can reduce Cu^{+2} to Cu^{+1} in an alkaline medium. The BCA protein assay combine Biuret reaction with the highly sensitive and selective colorimetric detection of the cuprous cation (Cu^{+1}) using a unique reagent containing bicinchoninic acid [46]. The chelation of BCA with cuprous ion can produce purple color and the complex exhibits a strong absorbance at 562 nm, which is linear with the protein concentration within the working range

(20-2000μg/mL). |Therefore protein concentration can be determined and calculated from the standard curve, which is usually drawn from a series of dilution of known concentration of bovine serum albumin (BSA).

2.5 Total organic carbon

Total organic carbon (TOC) is the amount of carbon found in an organic compound. There are three steps to measure TOC: (1) Total carbon (TC) measurement: Combustion and oxidation samples and all carbon present converts to carbon dioxide. The carbon dioxide generated by oxidation is detected using an infrared gas analyzer (NDIR). (2) Inorganic carbon measurement: the sample undergoes the sparging process, and the inorganic carbon (IC) in the sample is converted to carbon dioxide by acidification. (3) The TOC can be calculated by using the TC substrates IC. The TOC measurement principle is shown in Figure 2.7.

In this study, TOC measurement was used to test the polyethylene glycol (PEG) concentration in filtrated water. Commercially available PEG can have molecular weights ranging from 200 Da to tens of thousands of Da. Their separation and identification can be challenging due to the chemical diversity and complexity of the sample matrix and lack of a sufficient UV chromophore. Therefore TOC was used to determine the PEG concentration.

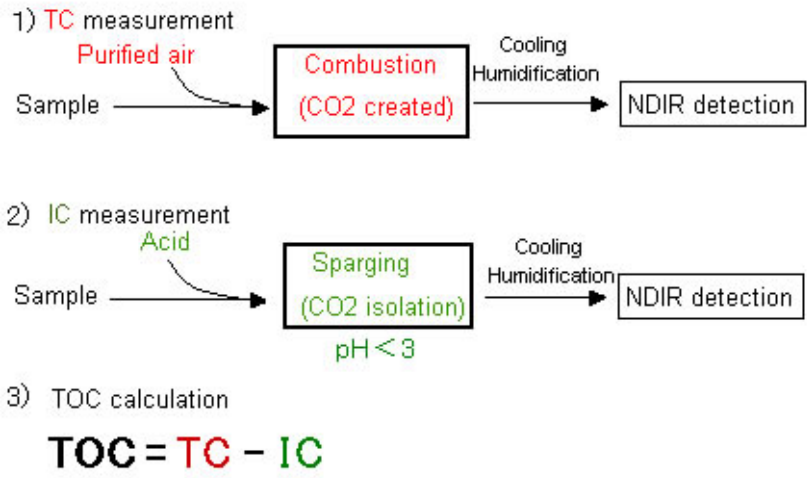

Figure 2.7. TOC measuremnt priciple [47].

Chapter 3 Fabrication of antifouling polyethersulfone (PES)/cellulose nanocrystals (CNC) nanocomposite membranes

3.1 Introduction

Polyethersulfone (PES) is an attractive polymeric material that is commonly employed for the preparation of porous microfiltration (MF) and ultrafiltration (UF) membranes. PES contains repeated units of ether and sulfone linkage alternating between benzene rings (Figure 3.1), and the unique structure endows PES remarkable properties including thermal stability, toughness, and resistance to mineral acids [48]. PES membranes are usually prepared by the phase inversion technique where , the polymer solution is subjected to a liquid-liquid demixing and solvent exchange with a non-solvent in a coagulation bath, and is solidified and separated into polymer-rich and polymer-lean parts, forming a solid polymer matrix and pores, respectively [49]. The PES membrane is widely utilized for water treatment in food, beverage, and medical industries [50].However, the inherent hydrophobic property of PES limits its application in membrane water treatment process [51]. It is well-known that the hydrophobicity of membranes causes their fouling due to the nonspecific solutes adhesion on membrane surface [52]. Fouling of membranes by various mechanisms including pore blocking and cake formation incurs flux decline due to the generation of extra resistance against transport of desired materials (here water) through the membrane. Therefore, the applied pressure must increase to compensated this flux reduction and membrane cleaning becomes necessary which both increase the operating cost of water treatment [53]. Fouling can also cause membrane degradation, resulting in shorter membrane lifetimes, and reduced selectivity of membranes [54]. Given that, modification of the current PES to mitigate fouling is the subject of ongoing research.

Many investigations have revealed that increasing membrane surface hydrophilicity can effectively reduce fouling [55]. There are four common approaches to increase PES membrane hydrophilicity: (i) grafting, including photo-induced grafting and thermal-induced grafting, (ii) surface coating, (iii) plasma treatment, and (iv) blending of hydrophilic materials with PES. Pieracci et al. [56] modified 10 kDa PES membrane by ultraviolet light-induced grafting with **N**-vinyl-2-pyrrolidinone. They showed that the hydrophilicity of membranes increased 25% and the BSA fouling decreased 49 %. Mu and Zhao [57] grafted poly(ethylene glycol) diacrylate (PEGDA) onto PES membrane surface by thermal-induced graft polymerization, which was accelerated by trifunctional trimethylolpropane trimethyl acrylate (TMPTMA). They reported enhanced permeability and antifouling properties after modification of membranes by surface grafting. Ma et al. [58] used an adsorption-crosslinking process to modify PES membrane by poly(vinyl alcohol) (PVA). The applied surface coating technique was reported to increase membrane surface hydrophilicity and flux recovery ratio, while the water flux decreased due to the formation of an extra layer on the PES membrane. Saxena at al. [59] exposed PES membrane to plasma of argon–oxygen ($Ar–O_2$) mixture. The membrane hydrophilicity was found to increase after plasma treatment, and thus less deposition of solute particles on the membrane surface and more water flux recovery ratio was observed. Although, surface grafting/coating and plasma treatment have been shown to effectively render the surface more hydrophilic, however, several disadvantages limits their application. First, these techniques are not easily implemented and thus their scaling up for large industrial application will be limited. Second, the chemicals used for grafting are typically environmentally unfriendly which raise environmental concerns [60].Third, grafted/coated materials on the surface can be easily leached out to the feed solution by cross-flow filtration in the case of weak interaction between these materials and the membrane surface. Fourth,

coated/grafted materials will add another resistance to the transport of materials passing through membranes and thus may adversely affect the permeation properties of the membranes.

Blending is a facile approach and easily scalable alternative for the modification of PES membranes. Hydrophilic polymers such as cellulose acetate [48], chitosan [61], PVP and PEG [62, 63] were common additives blended into casting solution to obtain improved hydrophilic property. The trend in the latest reports is to blend nanomaterials in the polymers to synthesize hybrid inorganic/organic membranes. Since most of these blended nanomaterials are hydrophilic in nature they all increased the hydrophilicity of the resulting membranes and thus improved their antifouling properties. The other advantages of synthesizing hybrid membranes are (i) increasing the water flux due to the larger effective surface area of membranes by nanomaterials and (ii) inducing the functional properties of the nanomaterials, e.g., antibacterial properties of TiO_2 and conductivity of indium tin oxide (ITO) [64], to the polymeric membranes. Integrating metal oxide nanoparticles such as single-element TiO_2 and SiO_2 and double element ITO into the porous membranes has been widely studied [64-67]. The aim of this study is to utilize a nanomaterial with different geometry, fibre-shaped cellulose nanocrystals (CNC) which is compatible properly with the polymer along the direction of its chains, to synthesize nanocomposite membranes.

Cellulose nanocrystals (CNC) are renewable [68], environmentally friendly [69] and nontoxic materials with high biocompatibility [70]. CNC also shows the properties of nanoparticles such as high mechanical strength [71]. The abundant hydroxyl groups from CNC is expected to improve the hydrophilicity of PES/CNC membranes [72]. In this study, CNC was used as an additive and blended with PES to prepare UF nanocomposite membranes. The influence of PES/CNC compositions on membrane performance and morphology was investigated and promising results in terms of permselectivity and antifouling properties were obtained.

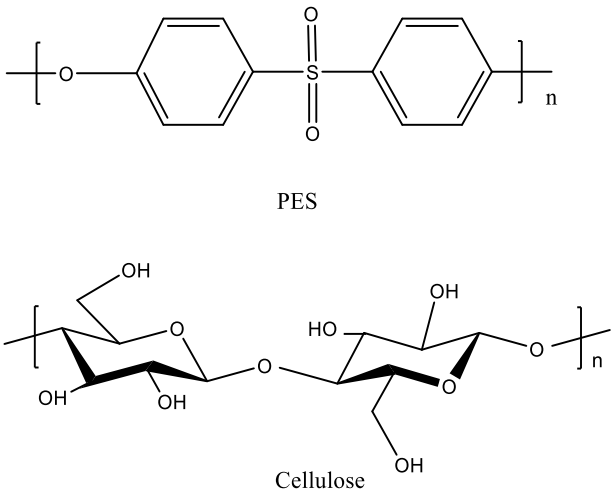

Figure 3.1. Molecular structures of polyethersulfone (PES) and cellulose

3.2 Materials and methods

3.2.1 Materials

Polyethersulfone (BASF PES Ultrason E6020P with *MW*= 75 kDa) and cellulose nanocrystals (CNC) with the particle length of 100-200 nm and the diameter of 5-15 nm, supplied by Alberta Innovates Technology Futures (AITF), were used for the preparation of membrane casting solution. *N*-methyl-2-pyrrolidone (NMP), polyethylene glycol (PEG, reagent grade, M_W = 0.6, 6, 10, 20 and 35 kDa), polyvinylpyrrolidone (PVP, reagent grade, M_W=10 kDa) and bovine serum albumin (BSA) were purchased from Sigma-Aldrich. Micro bicinchoninic acid (BCA) protein assay reagent kits were obtained from Pierce Biotechnology. Deionized water was used as the nonsolvent.

3.2.2 Preparation of membranes

Membranes were prepared by non-solvent phase-inversion method. PES and CNC were added into *N*-Methyl-2-pyrrolidone (NMP) solvent according to predetermined ratios (Table 3.1), followed by stirring at 300 rpm for 24 h at room temperature to obtain homogeneous solutions. Then the solutions were degassed in an ultrasonic bath for 10 min to remove air bubbles which may cause holes in prepared membranes. After degassing, the homogeneous solutions were cast on a glass

plate by a film applicator (Gradco). Casting speed was adjusted by a motorized film applicator (TQCAB3120) to 20 mm/s at room temperature. The thin cast films were finally immersed in the coagulation bath for 1 hour. Finally, the formed membranes were placed between two paper sheets and dried for 24 h at room temperature.

Table 3.1. Composition of casing solution and pore size of membranes.

Membranes	PES (Wt. %)	CNC (Wt. %)	NMP (Wt. %)	PVP (Wt. %)	MWCO (kDa)	Pore size (nm)
PES	15	0.00	83.00	2	68	12
PES/CNC 0.1 %	15	0.02	82.69	2	68	12
PES/CNC 0.5%	15	0.08	82.63	2	68	9
PES/CNC 1.0 %	15	0.15	82.55	2	35	9
PES/CNC 5.0 %	15	0.75	81.95	2	35	9

3.2.3 Contact angle

The water contact angle is an indicator of membranes surface wettability. The contact angle was measured by Rame-hart goniometer using sessile drop method [73]. 20 µl water drop was deposited onto the membrane surface by a syringe. To minimize the experimental error, contact angles at five different points of each sample were measured at room temperature and analyzed by ImageJ software. The average value of five spots was reported.

3.2.3 Water content

Membrane samples were cut into uniform size and the dry weights were recorded. Then they were soaked in distilled water for 24 h and weighed immediately after blotting to remove the free surface water. From wet and dry weights, the water content was obtained as follows:

$$Water\ content\ (\%) = \frac{W_w - W_d}{W_w} \times 100 \quad (1)$$

where W_w and W_d are the weights of wet and dry membranes (g), respectively [62]. The measurements were conducted three time and the average value of the results were reported to minimize the experiment error.

3.2.4 Flux, rejection and fouling evaluation

The pure water flux (PWF), protein rejection and water flux recovery ratio (FRR) were measured by a stirred Amicon cell (Model 8400, Millipore). The experimental setup is shown in Figure 3.2. The effective membrane area was 41.8 cm^2. All the experiments were carried out at the stirring speed of 250 rpm and the transmembrane pressure of 40 psi (applied by nitrogen gas). Each membrane was pre-compressed for 30 min to get stable filtration before all the measurements [74]. The pure water flux was calculated according to Eq. (2):

$$J_W = \frac{Q}{(A \times T)} \tag{2}$$

where J_W is the pure water permeation flux (L/m^2 hr or LMH); Q is the quantity of permeation (L); A is the effective membrane area (m^2); and T is the filtration time (hr.).

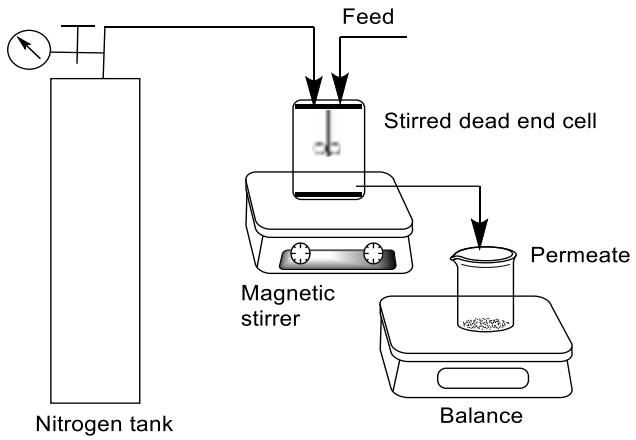

Figure 3.2 Setup for membrane permeation experiments.

BSA was used as a model protein for the rejection test. After the pure water flux measurement, the feed solution was replaced by 1000 mg/L BSA solution. The BSA concentration of the permeate

and the feed solution was measured with a bicinchoninic acid assay (assay) [75]. The membrane rejection (R) was calculatd as follows:

$$R(\%) = [1 - \left(\frac{C_p}{C_b}\right)] \times 100 \quad (3)$$

where C_p and C_b (mg/L) are the BSA concentrations in the permeate and the feed water solutions, respectively.

After BSA filtration, the membrane was washed by double distilled water for 30 min, and the pure water flux was measured again (J_{w2}) under the same condition as the first experiment. BSA filtration causes fouling problem due to the adsorption of protein on the membrane surface. The formation of BSA cake layer on the PES membrane decreases the water flux [76]. The antifouling capacity of membranes was expressed by calculating the FRR as follows:

$$FRR(\%) = \frac{J_w}{J_{w2}} \times 100 \quad (4)$$

where J_w and $J_{w2}$are the water flux before and after BSA filtration, respectively.

3.2.5 Pore size measurement

Pore size was semi-quantitatively estimated from molecular weight cut-off (MWCO). MWCO of membranes was determined by PEG with M_W range of 0.6-35 kDa. 1000 mg/L PEG solutions with different M_W were filtered by the dead end cell. The PEG concentration in the permeate and the feed solution was measured by a TOC analyzer (TOC-L CPH, Shimadzu, Japan). The relationship between pore size and MWCO are affected by many factors including steric and electrostatic, which can produce different results [77]. In this study, the relationship proposed by Lentsch et al. [78] was used to calculate the pore size from MWCO:

$$\mathrm{d} = 0.09 \times (MWCO)^{0.44} \quad (5)$$

where d is in nm and $MWCO$ is in Da.

3.2.6 Thermogravimetric analysis (TGA) measurements

The thermal stability of PES and PES/CNC blended membranes were measured by thermo-gravimetric analysis (TGA), which were carried out using a SDTQ600 (TA Instruments). Membranes were tested in air at a heating rate of 10 °C/min from 20 to 800 °C [79].

3.3 Results and discussion

3.3.1 Contact angle measurements

Contact angle is an effective indicator of membrane surface hydrophilicity. The smaller water contact angle, the higher surface hydrophilicity. The effect of CNC content in casting solution on membrane surface hydrophilicity is shown in Figure 3.3. The pristine PES membrane exhibited the highest contact angle of 66^{o}, corresponding to the lowest hydrophilicity. When the concentration of CNC in the casting solution increased to 5.0 wt. %, the contact angle gradually decreased to 43^{o}, indicating the surface hydrophilicity of membranes increased after blending CNC in the casting solution. The enhanced hydrophilicity of PES/CNC blended membranes can be attributed to the hydrophilic nature of CNC [80]. The lower hydrophilicity of the synthesized nanocomposite membranes is predicted to reduce the fouling of the membranes by mainly hydrophobic organic materials. More hydrophilic surface decreases the adhesion of hydrophobic organic molecules by moderating the effect of hydrophobic interaction. This assumption will be tested in the following sections.

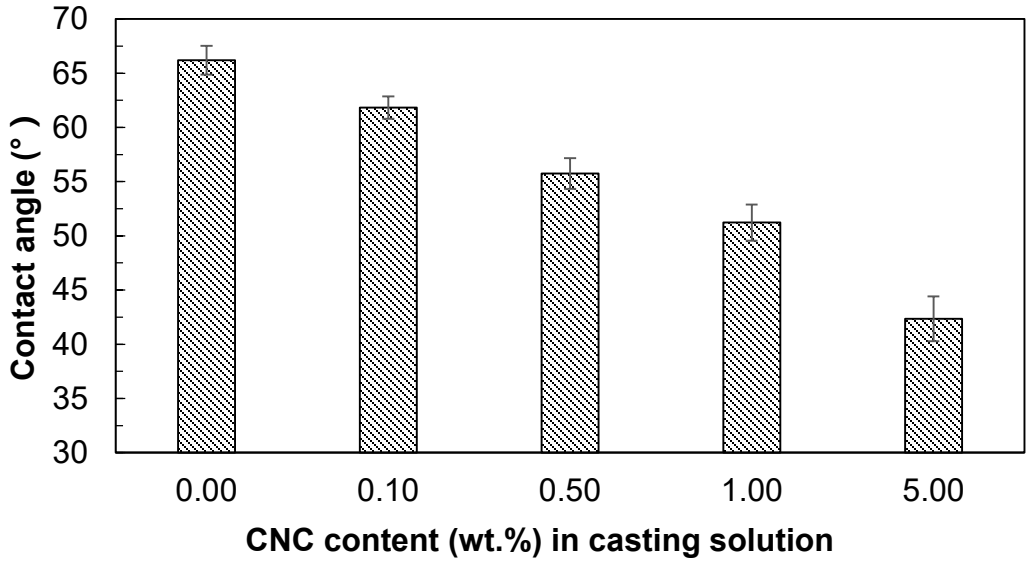

Figure 3.3. Contact angles of PES/CNC membranes as a function of CNC content.

3.3.2 Water content

Water content is another parameter that determines the hydrophilic/hydrophobic property of membranes. As shown in Figure 3.4, the water content enhanced by increasing the loading of CNC in the PES. The water content increased from 54 to 70% by blending 5.0 wt. % of CNC into casting solution, indicating the formation of a more hydrophilic membrane. The water content results also match well with contact angle data. As mentioned before, the increased water content is due to the hydrophilic character of CNC with abundant free hydroxyl groups [81].

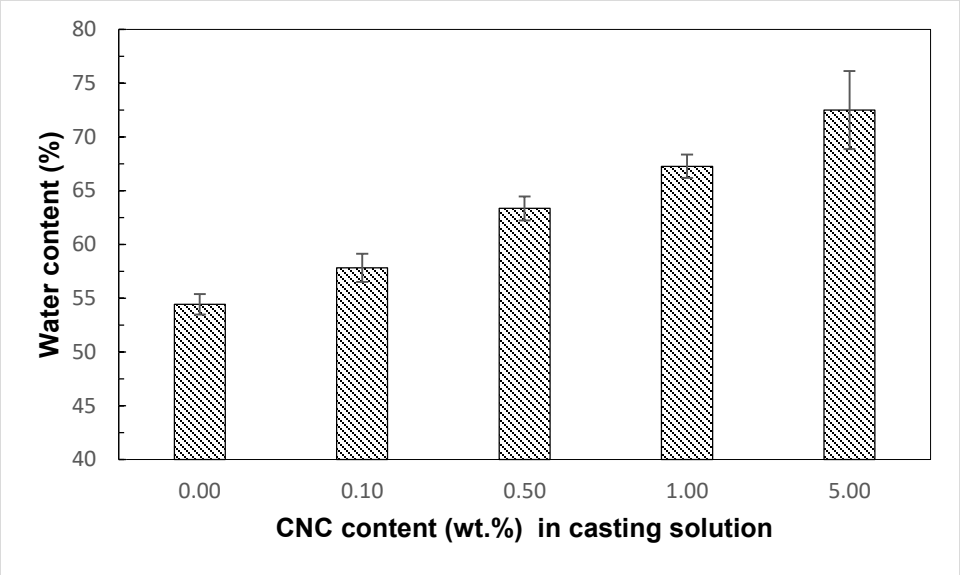

Figure 3.4. The water content of PES/CNC membranes as a function of CNC content.

3.3.3 Scanning electron microscopy morphological studies

The scanning electron microscopy (SEM) images were taken to study the effect of CNC on membrane morphologies (Figure 3.5). The pristine PES membrane (Figure 3.5 a) exhibits a typical asymmetric structure of non-solvent induced phase separation membranes with the finger-like structure of the cross-section. The asymmetric structure of the membrane comprised of a dense thin skin layer and a porous sub-layer. The interaction between components in the casting solution and phase inversion kinetics may change the membrane morphologies [82]. Two factors that may influence the thickness of membrane skin layer are as following:

(i) The increased concentration of CNC in the casting solution leads to increased viscosity of casting solution, which can hinder the exchange between solvent and non-solvent during the phase inversion and reduce the driving force for membrane precipitation. Consequently, the membrane skin layers become thicker [83];

(ii) Adding nanofillers into dope solution can make it thermodynamically unstable since less non-solvent (water) is needed to precipitate the polymer. In general, the hydrophilic

additives act like non-solvent, making the casting solution more unstable and thus lead to the formation of a thinner skin layer.

These two effects, i.e., kinetic hindrance and thermodynamic enhancement, contradict each other. The skin layer thickness of the membrane prepared with 0.5 wt. % CNC (Figure 3.5 b) is similar to the pristine PES membrane, and this is possibly because the two factors counteract each other. However, by the addition of more CNC (5.0 wt. % in Figure 3.5 e) the skin layer becomes thicker compared with unmodified PES membrane. This result can be attributed to the increased viscosity of casting solution at higher CNC loadings, which becomes the dominant influential factor of skin layer formation.

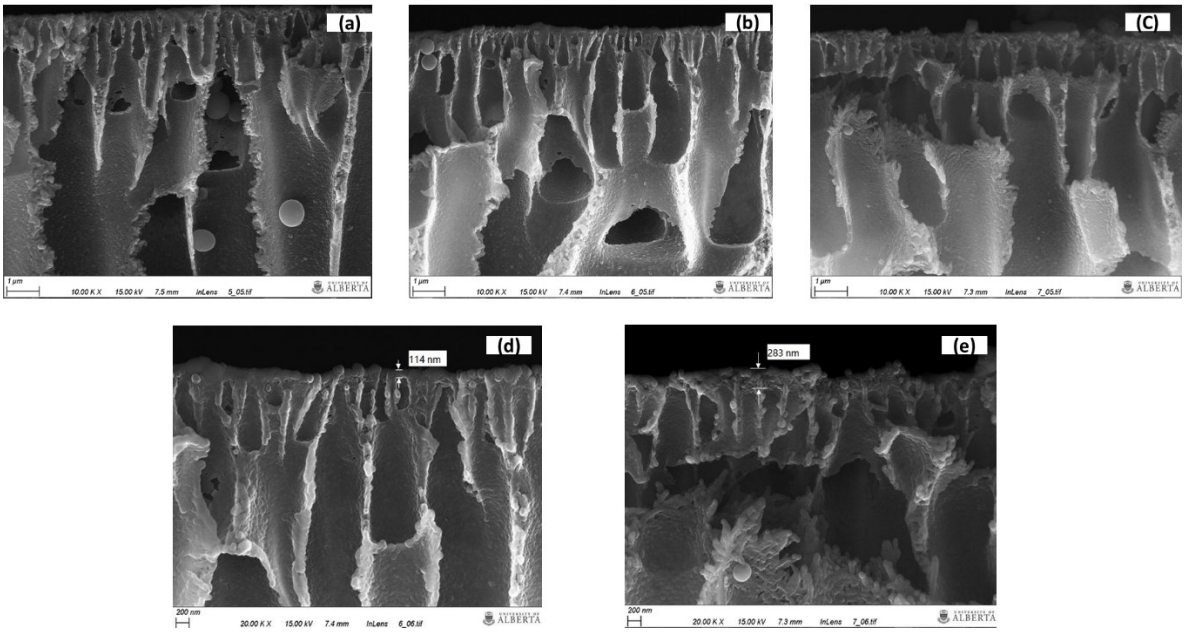

Figure 3.5. SEM cross-sectional images of PES/ CNC blended membranes:
(a) 0 wt. % CNC; (b) 0.5 wt. % CNC; (c) 5 wt. % CNC; and top-layer thickness of PES/CNC blended membranes: (d) 0.5 wt. % CNC; (e) 5 wt. % CNC.

3.3.4 Membrane performance

The influence of PES/CNC composition on PWF is shown in Figure 3.6. PWF of PES/CNC

blended membranes increased from 92 to 195 LMH with an increase in CNC concentration from 0 to 1.0 wt. % in the casting solution. The further increase of CNC content up to 5.0 wt. %, decreased the PWF to 168 LMH. In other words, there is an optimum amount of CNC that can lead to an increase in PWF through the membranes. The PWF is affected by pore size distribution, hydrophilicity, and the thickness of skin layer. Considering the effect of CNC on membrane properties, the hydrophilicity increased after blending CNC, which promotes membrane PWF. In contrast, high content of CNC in the casting solution resulted in smaller pore size and thicker top layer, which can decrease PWF. The PWF through PES/CNC membranes is controlled by a trade-off relationship between thses parameters. It was enhanced by increasing the CNC content up to 1.0 wt. %, indicating that the increased hydrophilicity was the primary factor, and decreased by further addition of the CNC up to 5 wt. %, implying that the effect of pore size and skin layer thickness became domniant.

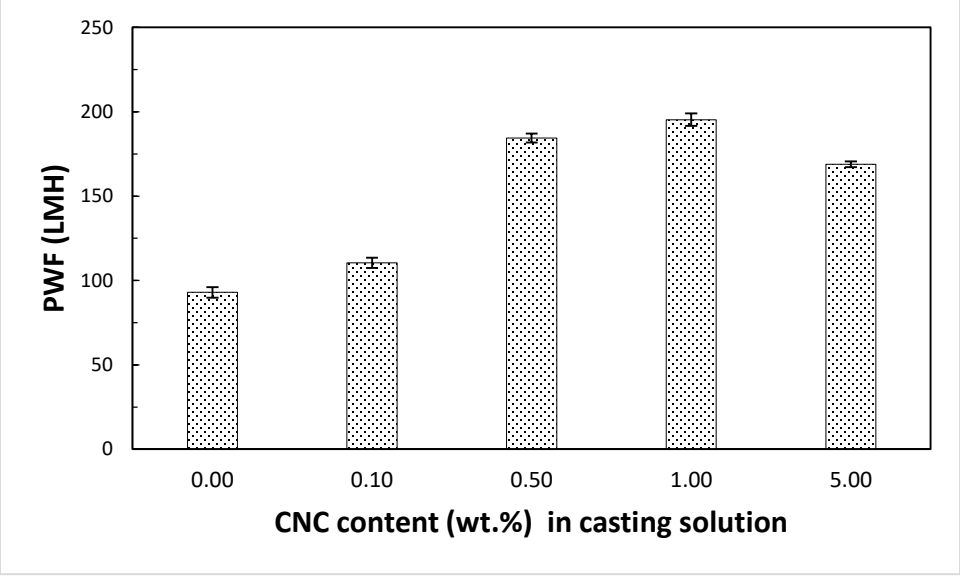

Figure 3.6. Effect of PES/CNC composition on membrane pure water flux.

BSA rejection ratio (Figure 3.7) enhanced from 93 (pristine membrane) to 96 and 97% when 1.0 and 5.0 wt. % CNC were added into the PES casting solution, respectively. BSA rejection ratio is

mainly affected by the membrane pore size, and the smaller pore size resulted in higher BSA rejection ratio [84]. Hence, the addition of CNC improved the quality of the permeate water quality (BSA rejection), as well as its recovery rate (PWF).

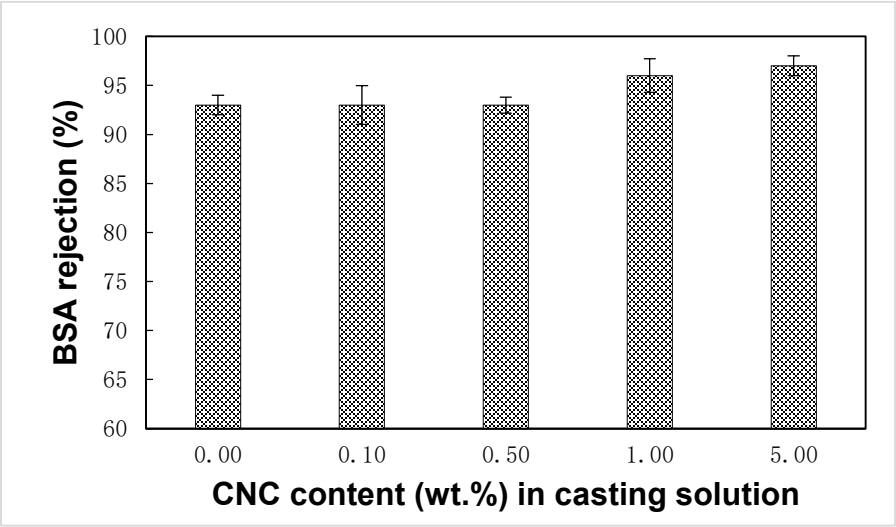

Figure 3.7. Effect of PES/CNC composition on membrane BSA rejection.

3.3.5 Antifouling properties

Membrane fouling can result in reduced water flux, which is caused by the deposition and adsorption of proteins on the membrane surface. The antifouling property of the synthesized membranes was studied by ultrafiltration of BSA/water solutions and is expressed by FRR which is a criterion for membrane antifouling capacity. As shown in Figure 3.8, the FRR enhanced from 51 to 90% when CNC content increased from 0 to 5.0 wt. % in the casting solution, indicating the significant improvement in antifouling property of PES/CNC nanocomposite membranes. This result can be attributed to the improvement of membrane hydrophilicity [74]. It is generally accepted that increasing the hydrophilicity of the membranes provided better fouling resistance as most foulants (here protein) are hydrophobic in nature.

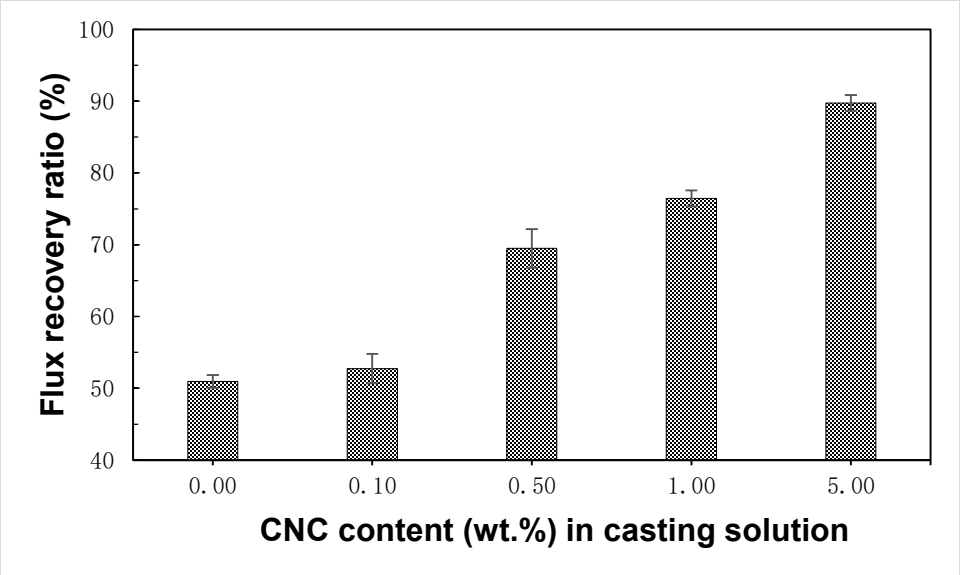

Figure 3.8. Effect of PES/CNC composition on membrane flux recovery ratio.

3.3.6 Thermal properties of PES and PES/CNC blended membranes

TGA curves of CNC, pristine membrane, and PES/CNC nanocomposite membranes are shown in Figure 3.9. The decomposition temperature is defined as the temperature where 3% weight loss occurs [38]. It was found that the decomposition temperature decreased with increasing the amount of CNC in the polymer matrix. The decomposition temperature of PES membrane decreased from 467 to 260 °C when 5.0 wt. % CNC was used. The lower decomposition temperature of CNC resulted in the diminished thermal stability of the blended membranes. Although the thermal stability decreased after blending CNC, the nanocomposite membranes were found to be stable at temperatures up to 260 °C indicating that these membranes can still meet the thermal stability requirement of water treatment in various applications. Thus the outstanding permeation and antifouling properties of the synthesized PES/CNC nanocomposite membranes can easily compensate the decreased thermal stability that makes these membranes favorite for protein separation from water.

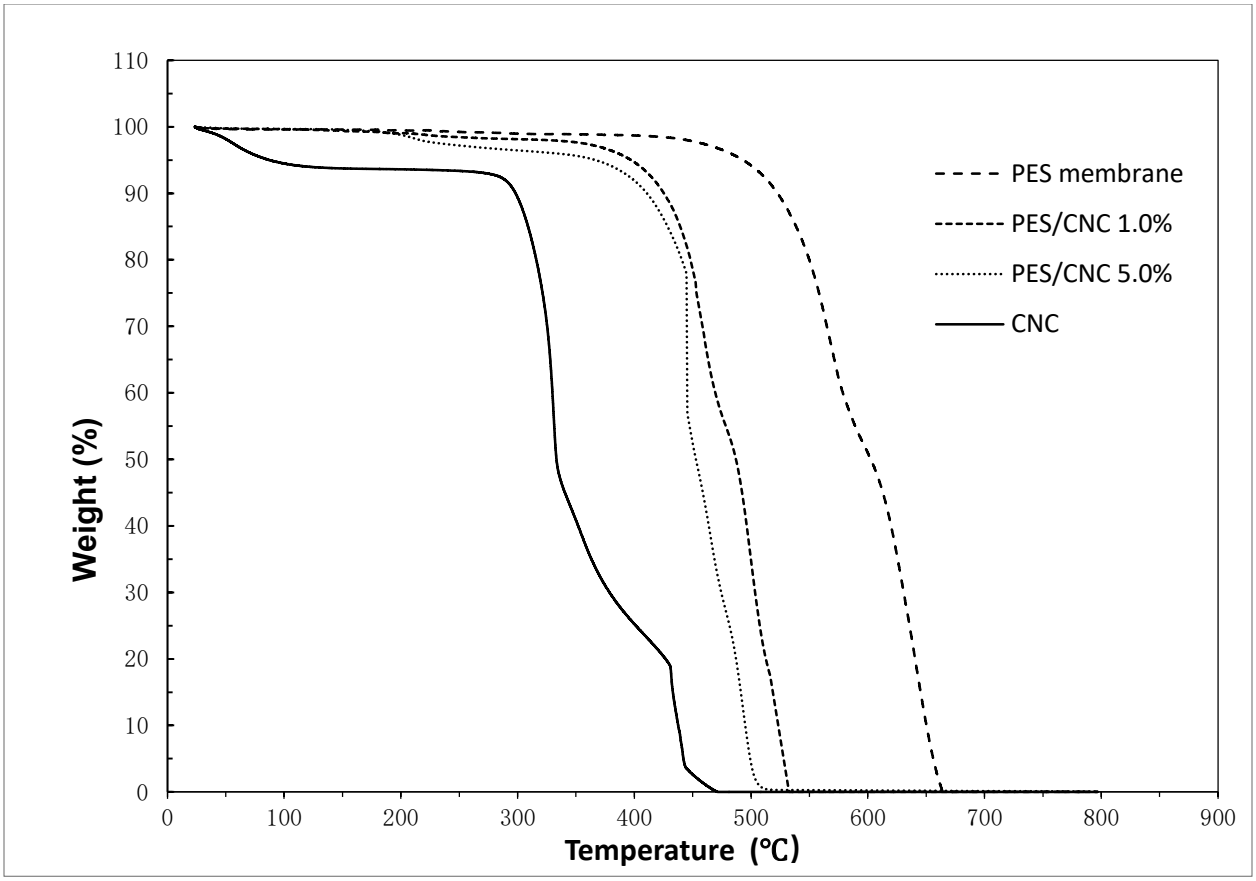

Figure 3.9. TGA curve of CNC and PES/CNC membranes.

3.4 Conclusion

PES/CNC nanocomposite membranes were prepared by blending different amount of CNC, as renewable and potentially safe nanomaterial. The effect of CNC content in casting solution was investigated. The contact angle and water content results revealed that the hydrophilicity of the membranes enhanced significantly by increasing the CNC content in the casting solution. The pure water flux was improved with an increase of CNC concentration up to 1.0 wt. %, and decreased with further addition of CNC in the casting solution up to 5.0 wt.%. BSA rejection was also improved by increasing CNC content due to the formation of smaller pore size and thicker skin layer of the nanocomposite membranes. The antifouling property was significantly improved after

blending CNC as quantified by measuring the flux recovery ratio. Finally, the thermal stability of PES/CNC nanocomposite membrane was found to be lower than unmodified PES membranes. The synthesized nanocomposite membranes have a high potential to be used for cost- and energy-efficient removal of protein from wastewater.

Chapter 4 Flocculation and dewatering of mature fine tailings using temperature-responsive cationic polymers

4.1 Introduction

The huge volume of undesired tailings produced during the bitumen extraction process are raising environment concerns. Large area of tailing ponds is required to store those tailings, in which the tailings separate into three layers after settling for several months. The heaviest coarse sands settle to the bottom and water released from tailings form the top layer. The middle layer, which contains fine clays, water and residual bitumen, is known as mature fine tailings (MFT). MFT forms "gel-like" suspensions with particles of sizes smaller than 44 μm [2]. Due to the small particle size and high water retention capacity [3], MFT suspensions take several years to settle and release the entrapped water.

In the past decades, several studies have been conducted by many researchers in order to accelerate the settling rates of MFT and enhance the water recovery rates. There are some techniques such as natural process, biological treatment, physical/mechanical process, and chemical treatment. (1) Natural process, such as the freeze-thaw process occurs when tailings are frozen in winter and then thawed in the following summer. It has been reported that the solids content of MFT increased from 30% to around 45% after freeze-thaw treatment [5]. Although the cost of freeze-thaw method is low, the drawbacks of this method are labor intensive and time consuming; (2) Biological treatment: suitable species are planted on the high water content tailings, and the dewatering is achieved by transpiration through the leaves and root system [6]. However, the high saline and sodic tailings limit the species that can be applied, and this method is also dependent on local

weather and climate conditions; (3) Physical/mechanical processes include filtration [8], centrifuge [9], and electrical treatment [10-12]. The most traditional one is filtration, which has low environmental impacts while the cost is relatively high. Centrifuge is another common method, and it has been reported that this method can produce tailings with around 60% solid contents. Centrifuge requires relatively small storage area and can recover large amount of water, while the cost is high and requires experienced operators. The third method is electrical treatment. The working principle of electrical treatment is applying direct current (DC) electric field to the negatively charged particles, thus the particles will move to the positive (anode) electrode, leading to higher settling rate; (4) Chemical treatment, such as coagulants and flocculants. In particular, chemical treatment has gathered the most attention because it is high efficiency. Coagulants like gypsum can introduce calcium cations to neutralize negative charged particles and reduce the repulsion between particles. Synthetic polymers are also useful for effective flocculation, and it is one of the most widely used methods to dose polymer flocculants into MFT suspension to bridge the fine particles and subsequently flocculate these particles into big flocs. Researchers have synthesized inorganic/organic hybrid polymeric flocculants such as $Al(OH)_3$-polyacrylamide (Al-PAM) to accelerate the settling rate and enhance dewatering. The cationic nature of imbedded aluminum hydroxide can improve the performance of polyacrylamide (PAM) [13-16]. Recently, temperature-responsive poly(*N*-isopropylacrylamide) (PolyNIPAM) has been reported as novel flocculant to accelerate settling rate and enhance consolidation [17-22]. PolyNIPAM can adsorb onto the particle surface at temperature below the LCST via hydrogen bonding interactions. By increasing the temperature above the LCST, the polymers experience a phase transition and become hydrophobic, resulting in the collapse of polymer chains. As a result, particles in tailings suspension are rapidly flocculated and settled due to those strong hydrophobic interactions. Li et

al. [17] studied the adhesion force between kaolin particles and polyNIPAM by AFM. The results showed that the adhesion force increased from almost zero to 3.5 mN/m by increasing temperature from room temperature to 40 °C, and the repulsion between particles decreased to almost zero after increasing temperature. Once the big flocs were formed, the sediment was cooled below the LCST so the polymer become hydrophilic again and detach from particles, thus small particles can fill the gap between flocs to further enhance consolidation [23-25]. However, the nonionic property of polyNIPAM limits its application due to failure to neutralize some charged particles [19, 26]. To further improve the performance of polyNIPAM, several research groups have focused on introducing cationic groups to polyNIPAM in order to achieve higher flocculation ability [27]. Lu et al. [18] has synthesised polyNIPAM based copolymer poly(AEMA51-*st*-MAAmBo76-*st*-NIPAM381) containing 2-aminoethyl methacrylamide hydrochloride (AEMA) and 5-methacrylamido-1,2-benzoboroxole (MAAmBo) to increase the settling rate and water clarity of clay suspension. The copolymer showed higher settling rate as a result of the stronger electrostatic forces between positively charged polymer and negatively charged particle.

In this study, temperature responsive polyNIPAM and its copolymer poly(AEMA-*st*-NIPAM) were synthesised by free-radical polymerization. PolyNIPAM were mixed with poly(acrylamide-co-diallyldimethylammonium chloride) (poly(AAm-co-DADMAC)) at five different ratio to determine the optimum ratio for MFT flocculation and dewatering. The initial settling rate (ISR), supernatant turbidity, water recovery ratio and solid content were measured to determine the effect of different polymers and dosages on MFT solid-liquid separation.

4.2 Materials and methods

4.2.1 Materials

N-Isopropylacrylamide (NIPAM) monomer, poly(acrylamide-co-diallyldimethylammonium

chloride) (poly(AAm-*st*-DADMAC)), ammonium persulfate (APS), and tetramethylethylenediamine (TEMED) were purchased from Sigma-Aldrich Chemicals (Oakville, ON, Canada). NIPAM monomer was purified in benzene, and recrystallization was performed in hexane. 2-Aminoethyl methacrylamide hydrochloride (AEMA) monomer was synthesized following the reported procedure [21].

4.2.2 Synthesis of linear statistic polyNIPAM and poly(AEMA-*st*-NIPAM)

The homopolymer polyNIPAM was synthesized by conventional free-radical polymerization. 2 g of purified NIPAM monomer and 10 mg APS were dissolved in 40 mL DI water, followed by addition of 25 μL TEMED. The solution was degassed for 30 min under nitrogen. The reaction was kept at room temperature for 24 hours followed by dialysis against DI water for 3 days and then freeze-dried. The synthesis of copolymer poly(AEMA-*st*-NIPAM) was similar to the procedure of polyNIPAM. 1.67 g NIPAM monomer, 0.37 g AEMA monomer and 10 mg were dissolved in 40 mL DI water, followed by addition of 25 μL TEMED. The solution was degassed for 30 min under nitrogen. The reaction was kept at room temperature for 24 hours followed by dialysis against DI water for 3 days and then freeze-dried.

4.2.3 Characterization of polymers

Proton nuclear magnetic resonance (^{1}H NMR) spectra was recorded on a Varian 500 MHz spectrometer using D_2O as the solvent. Polymer lower critical solution temperature (LCST) as determined by UV-vis at 500 nm. 0.1 wt. % polymer was dissolved in DI water and heated from 20 to 60 °C at the rate 0.5 °C/min. The transmittance was continuously recorded during the temperature increase process. The LCST is determined as the temperature which the transmittance decreased to 50%.

4.2.4 Settling test

Mature fine tailings (MFT) suspension at 10 and 15 wt. % were prepared by dilution of 39 wt. % MFT with oil sands process water (OSPW). Different polymers were dissolved in DI water in a predetermined concentration, and mixed according to five difference ratios and stirred overnight. MFT suspensions were stirred for 2 min in a 250 mL beaker followed by addition of polymer solutions at the rate of 0.1mL/s. The stirring was stop after the addition of polymer solution. The settling tests were conducted in 100 mL graduated cylinders. The cylinder was inverted three times and left still on the bench at 25 °C, and the mudline height (the interface of supernatant and sediment) was recorded as a function of time. For the settling test under 50 °C, the polymer solution was added to MFT suspension under room temperature and followed the same stirring condition as the batch of 25 °C. Then the mixture was heated to 50 °C and started to record the mudline height as a function of time.

The initial settling rate (ISR) was calculated by plotting the mudline height versus time. The slope of linear part was considered as ISR. After 24 hours settling, the supernatant was carefully removed by a glass transfer pipette, and the transmittance of supernatant was measured at 4 °C by UV-vis at 500 nm wavelength. The turbidity (NTU) of supernatant was calculated from the equation NTU $\approx 0.191+926.1942\times[-\log(\%T/100)]$ [18], where %T is transmittance. After remove the supernatant, the sediment of was filtered and dried at 70 °C for 24 h. The sediment solids content was determined by dividing the mass of dry sediment by the total mass of sediment. The water recovery was determined by dividing the volume of water released by the total volume of MFT suspension.

4.3 Results and discussion

4.3.1 Synthesis of polymers

Linear NIPAM homopolymer and statistic copolymer based on NIPAM and 2-aminoethyl methacrylamide (AEMA), poly(AEMA-*st*-NIPAM), were synthesized by conversional free-radical polymerization for solid-liquid separation. Monomer AEMA containing protonated amino group was introduced into the copolymer in order to increase the interaction between particles and polymers via electrostatic force. The composition of copolymer poly(AEMA-*st*-NIPAM) was determined by ^{1}H NMR (Figure 4.1).

Lower critical solution temperature (LCST) of polyNIPAM and poly(AEMA-*st*-NIPAM) were determined by UV-vis spectrometer at 500 nm wavelength with a heating rate of 0.5°C/min. LCST of polymers is defined as the temperature at which the light transmittance decreased to 50%. The results are shown in Figure 4.2. The LCST of NIPAM homopolymer was found to be around 33 °C, which is in good agreement with previous reports [85-87]. LCST of poly(AEMA-*st*-NIPAM) copolymer was around 45 °C. The increased LCST of copolymer poly(AEMA-*st*-NIPAM) can be attributed to the hydrophilic property of AEMA. The increased hydrophilicity will facilitate the interaction between polymers and solvent [88, 89], resulting in increased LCST.

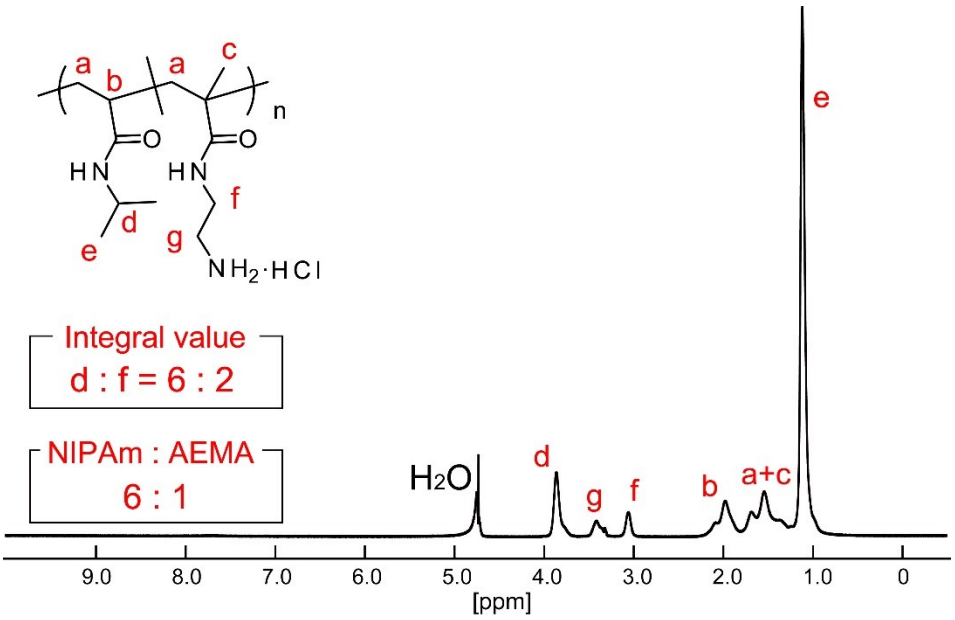

Figure 4.1. ^{1}H NMR spectra for poly(AEMA-*st*-NIPAM)

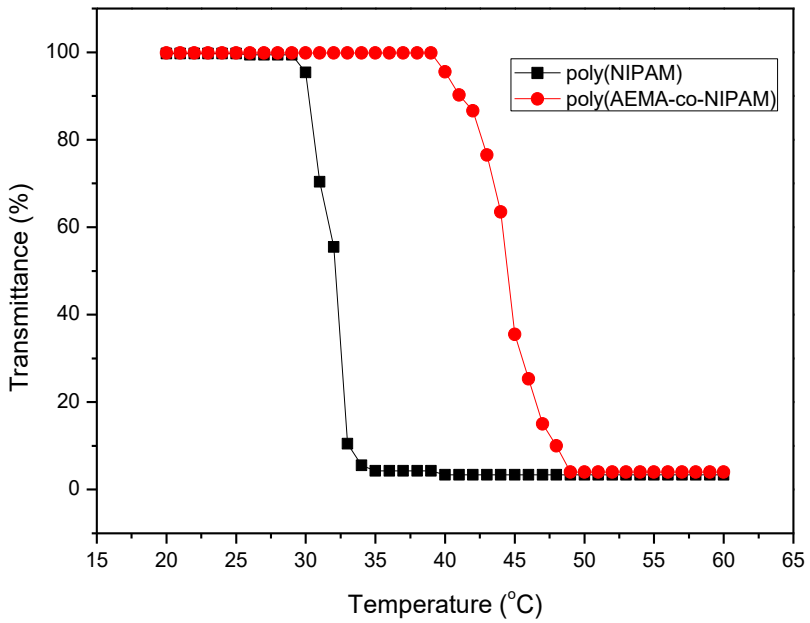

Figure 4.2. Lower critical solution temperatures (LCSTs) of polyNIPAM and poly(AEMA-*st*-NIPAM)

4.3.2 Initial settling rates (ISR)

The results of initial settling rates of 10 wt. % MFT are shown in

.

. Poly(AAm-co-DADMAC) (**D10**) (

.

a) cannot achieve ISR higher than 1 m/s for all three dosages (500, 750 and 1000 ppm), and ISR at 50 °C were the same as the ISR at 25 °C as poly(AAm-*st*-DADMAC) is not temperature responsive to temperature. The relatively low ISR may due to the insufficient bridging force to capture a large amount of particles. After mixing with polyNIPAM, ISR gradually increased until polyNIPAM content reach 70% (wt/wt) (

.

d, **D3N7**). While ISR of 10 wt. % MFT treated by polyNIPAM alone (**N10)** (

.

e) were decreased slightly compare to **D3N7**, and the decreased ISR may be due to the overdosed polyNIPAM flocculants. It is general accepted that settling rates keep increase with addition of polymer flocculants until reaching the optimum dosage. Addition more polymers flocculants results in decreased ISR [90]. According to the equation $P_B = \theta(1-\theta)$ where P_B is the probability of polymer cover on particles and θ is the particle surface covered by polymer flocculant [18]. P_B can reach maximum when θ is 0.5, indicating that the highest ISR can be achieve when half of the particle surface is covered by flocculants. When more than 50% of the particle surface is covered, there will be less free space left for polymers to attach. In addition, the overlap of mushroom or brushes from the overdosed polymers can cause steric hindrance and further impede particle attachment [91], resulting in decreased ISR. MFT treat by poly (AEMA-*st*-NIPAM) (PAN)

(

.

f) can achieve relatively high ISR which can be explained by the electrostatic interaction between negatively charged particles and the positively charged polymer. Compared to ISR at 25 °C, higher ISR were observed at 50 °C, and the increased ISR is resulted from the hydrophobic force from polyNIPAM at the temperature above LCST. Moreover, higher temperature can reduce system viscosity, leading to more homogenous distribution of polymers thus further promotes polymer adsorption onto particle surface [92]. The summary results 10 wt. % MFT dosed by different polymers is shown in a 3D figure (Figure 4.4). In general, the higher composition of polyNIPAM is needed to significantly improve ISR.

As for the case of 15 wt. % MFT (Figure 4.5), ISR were much lower than 10 wt. % MFT. Alamgir et al. [14] have proposed Al-PAM assisted filtration system, which also only worked for MFT diluted to up to 10 wt. %, and there was no visible enhancement of dewatering for MFT with 15 wt. % solids. In our study, the highest ISR of 15 wt. % MFT suspension can reach around 0.3 m/s, while the settling rate for control group is 0 within 24 hours. The summary results 15 wt. % MFT dosed by different polymers is shown in a 3D figure (Figure 4.6). Compared with 10 wt. % MFT, higher dosage is required for 15 wt. % MFT to achieve fast settling rate.

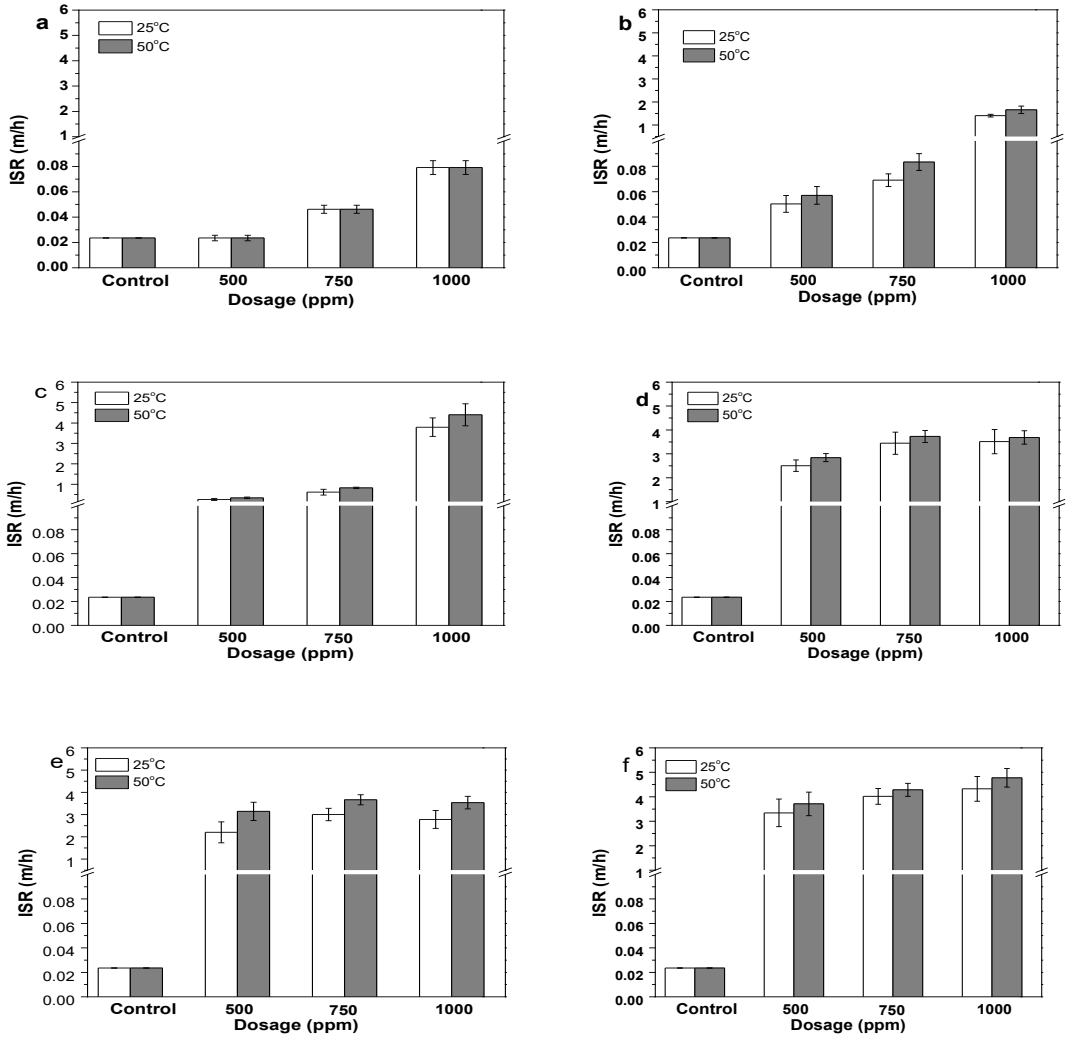

Figure 4.3. Initial settling rates (ISR, m/h) of 10 wt. % MFT treated by:

(a) poly(AAm-*st*-DADMAC) (**D10**), (b) mixture of 70% (wt./wt.) poly(AAm-*st*-DADMAC) and 30% (wt./wt.) polyNIPAM (**D7N3**), (c) mixture of 50% (wt./wt.) poly(AAm-*st*-DADMAC) and 50% (wt./wt.) polyNIPAM (**D5N5**), (d) mixture of 30% (wt./wt.) poly(AAm-*st*-DADMAC) and 70% (wt./wt.) polyNIPAM (**D3N7**), (e) polyNIPAM (**N10**), (f) poly(AEMA-*st*-NIPAM).

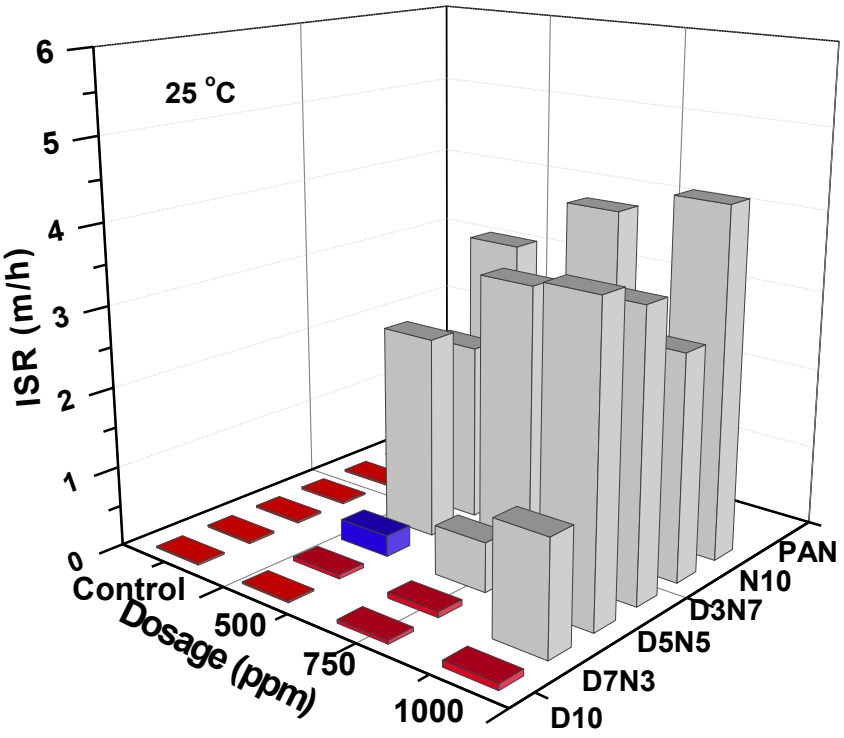
25 °C
ISR (m/h)
0
1
2
3
4
5
6
Control
500
750
1000
Dosage (ppm)
PAN
N10
D3N7
D5N5
D7N3
D10

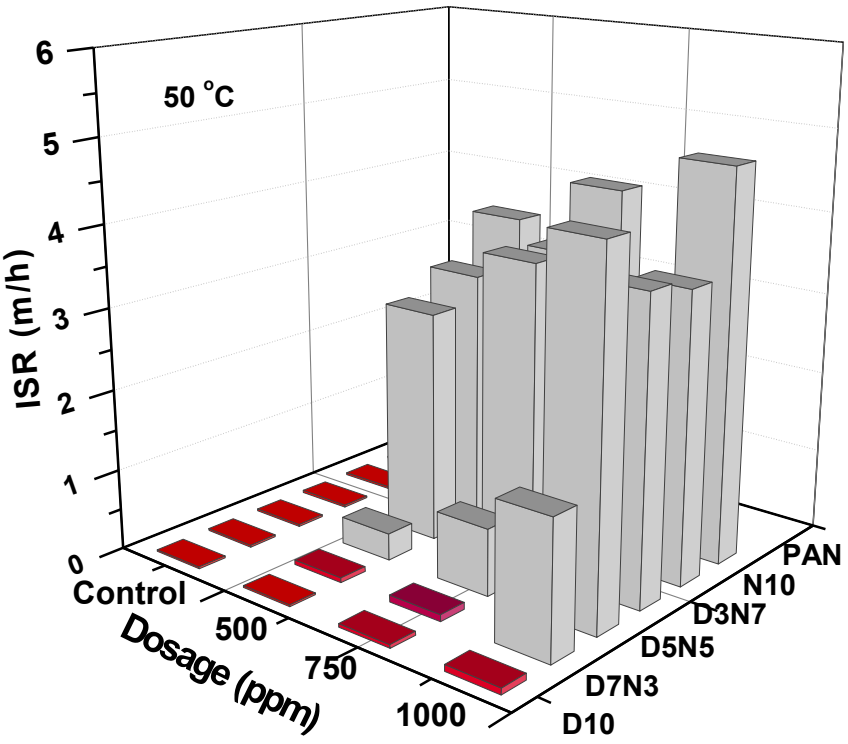

.

Figure 4.4. 3D graph of ISR of 10 wt. % MFT at 25°C and 50°C.

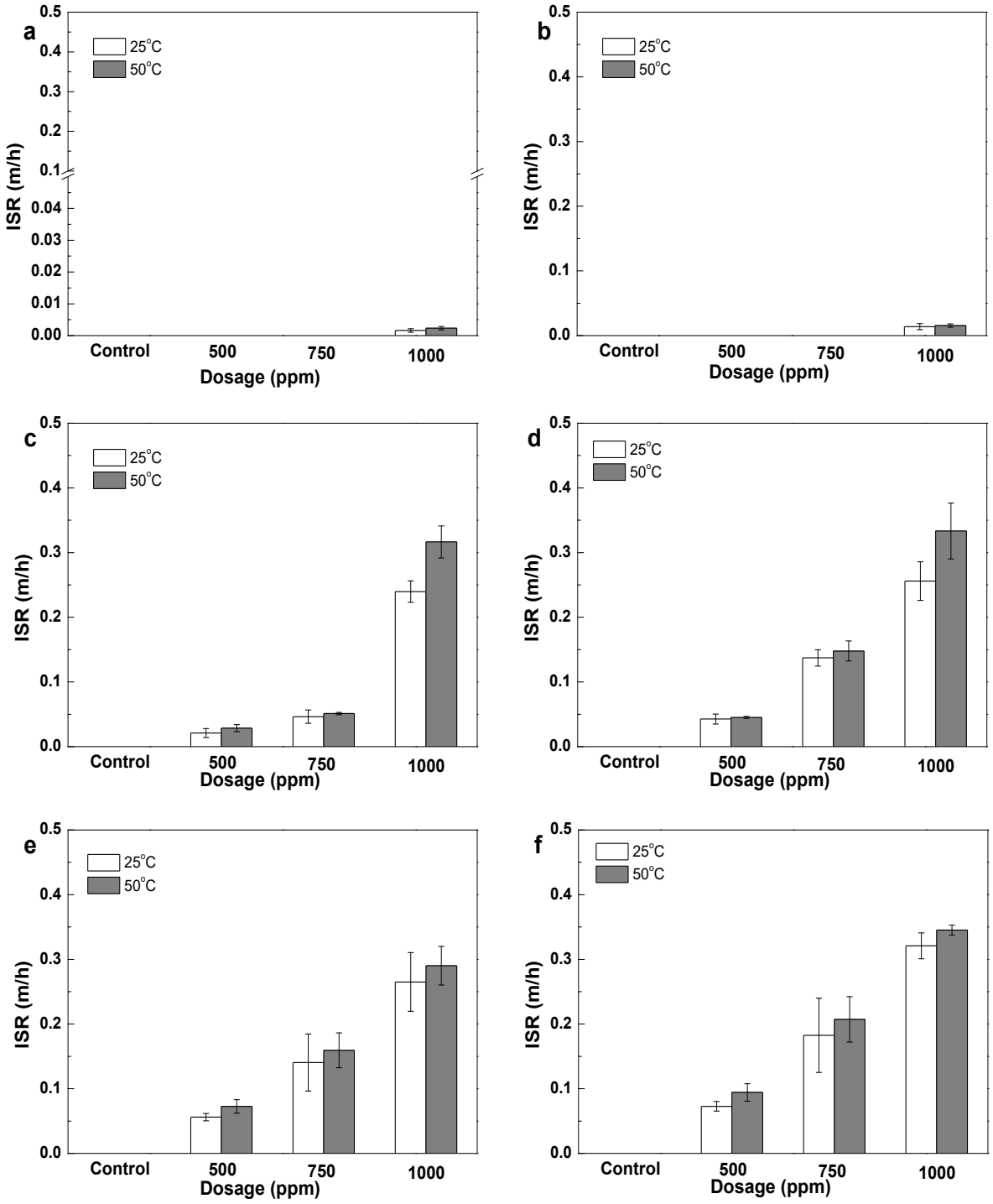

Figure 4.5. Initial settling rates (ISR, m/h) of 15 wt. % MFT treated by:

(a) poly(AAm-*st*-DADMAC) (**D10**), (b) mixture of 70% (wt./wt.) poly(AAm-*st*-DADMAC) and 30% (wt./wt.) polyNIPAM (**D7N3**), (c) mixture of 50% (wt./wt.) poly(AAm-*st*-

DADMAC) and 50% (wt./wt.) polyNIPAM (**D5N5**), (d) mixture of 30% (wt./wt.) poly(AAm-*st*-DADMAC) and 70% (wt./wt.) polyNIPAM (**D3N7**), (e) polyNIPAM (**N10**), (f) poly(AEMA-*st*-NIPAM).

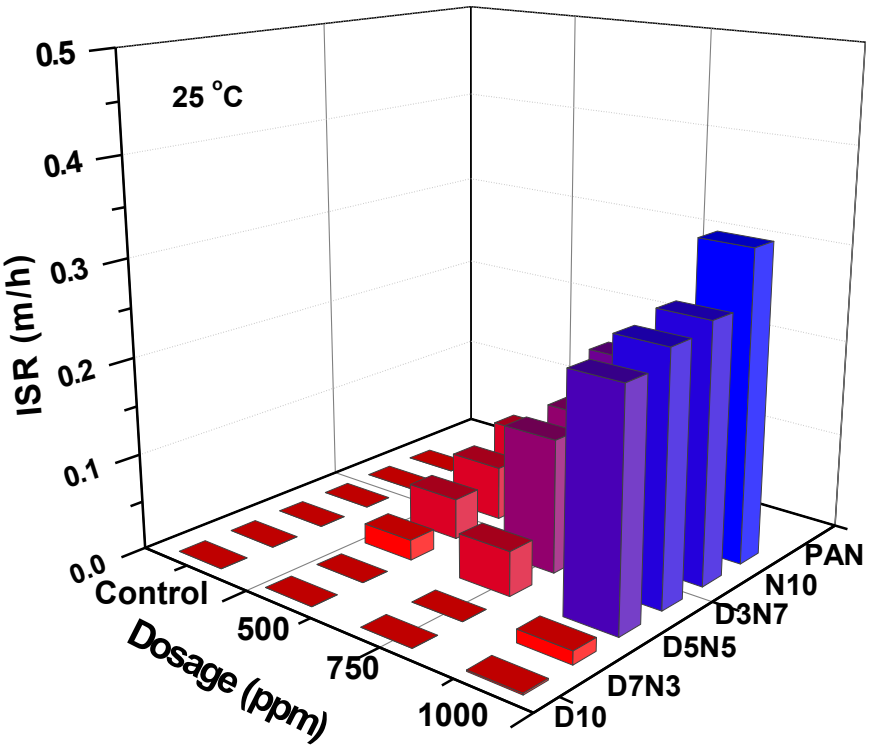

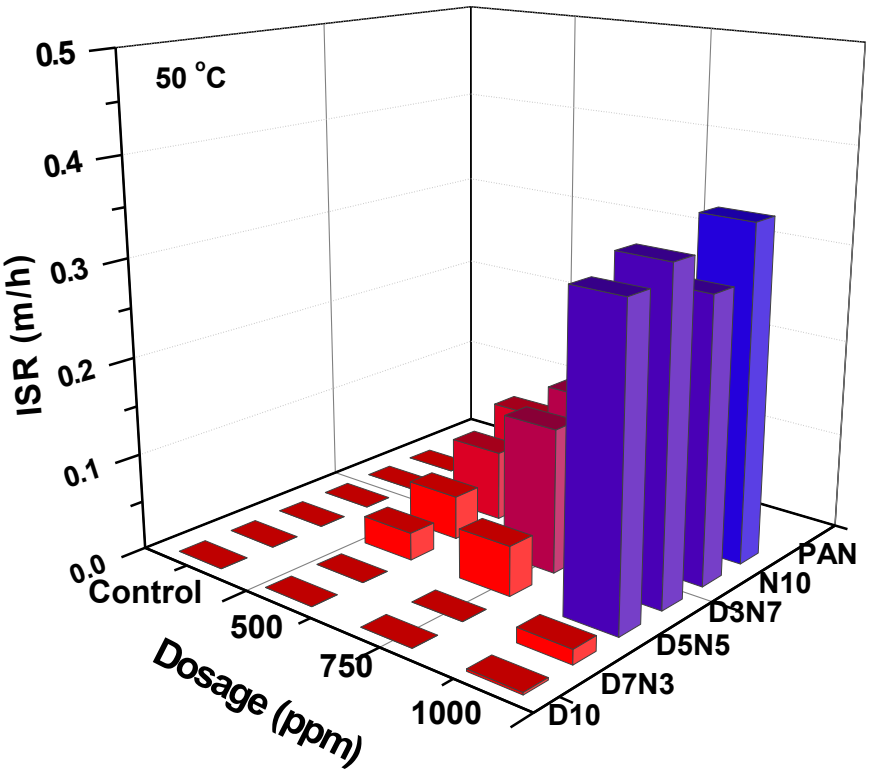

Figure 4.6. 3D graph of ISR of 15 wt. % MFT at 25°C and 50°C.

4.3.3 Supernatant turbidity

The supernatant turbidity of 10 wt. % MFT is shown in Figure 4.7. Poly(AAm-co-DADMAC) (D10) (Figure 4.7 a) can achieve lowest turbidity after 24 hours settling. Although D10 showed lowest ISR and highest mudline height (data not shown), D10 produced clear supernatant by neutralization of fine negative charged particles. 10 wt. % MFT suspension treated by D7N3 (Figure 4.7 b) and D5N5 (Figure 4.7 c) also showed relatively low turbidity. However, when the component of poly(AAm-st-DADMAC) decreased to 30% (D3N7, Figure 4.7 d), the turbidity significant increased maybe because 30% (wt./wt.) poly(AAm-st-DADMAC) is not sufficient to neutralize all negative charged particles, and electrostatic repulsion between negative charged

particles can promote the stability of suspension, leading to low clarity of supernatant. The 10 wt. % MFT treated by N10 (Figure 4.7e) showed the highest turbidity and even higher than the control group as neutral polyNIPAM failed to neutralized the negative charged fine particles. On the other hand, the polyNIPAM used in this study was prepared by conventional free-radical polymerization and as the molecular weight distribution is large some polyNIPAM with low molecular weight may work as dispersant and provide steric repulsion between particles [93], leading to poor clarity of supernatant. Increasing the polyNIPAM dosage decreased even further the clarity of supernatant. Therefore, for 10 wt. % MFT, D5N5 (c) is the optimum ratio to achieve both high ISR and low turbidity. 10 wt. % MFT treated by poly(AEMA-st-NIPAM) can also produce high clarity of supernatant (Figure 4.7 f). The cationic AEMA residues can neutralize negative charged fine particle thus increasing the clarity of released water. The protonated AEMA residues in poly(AEMA-st-NIPAM) can also enhance the adhesion of onto the particle surface by electrostatic force thus the flocculation effects can be further improved. The summary turbidity results of 10 wt. % MFT is shown in a 3D figure (Figure 4. 8). **D10, D7N3** and **D5N5** those three polymer solutions shown lower turbidity compared to the other groups.

Figure 4.9 a shows the turbidity of 15 wt. % MFT suspension treated by 1000 ppm D10, D7N3 and D5N5 (no water released within 24 h for these three groups if the dosage lower than 1000 ppm). In general, these three groups can achieve high clarity with turbidity around or lower than 100 NTU. D3N7 (Figure 4.9 b) showed slightly higher turbidity, following similar trend as 10 wt. % MFT. While the case of N10 (Figure 4.9 c) exhibited significantly higher turbidity, and 15 wt. % MFT treated by 1000 ppm N10 polymers solution even reached 500 NTU turbidity, which may result from the failure of neutralization negative charged fine particles. Poly(AEMA-st-NIPAM) can also produce lower turbidity of supernatants for the case of 15 wt. % MFT, which can be

attributed to the neutralization of negative charged particles and stronger adhesion of the cationic charged polymers.

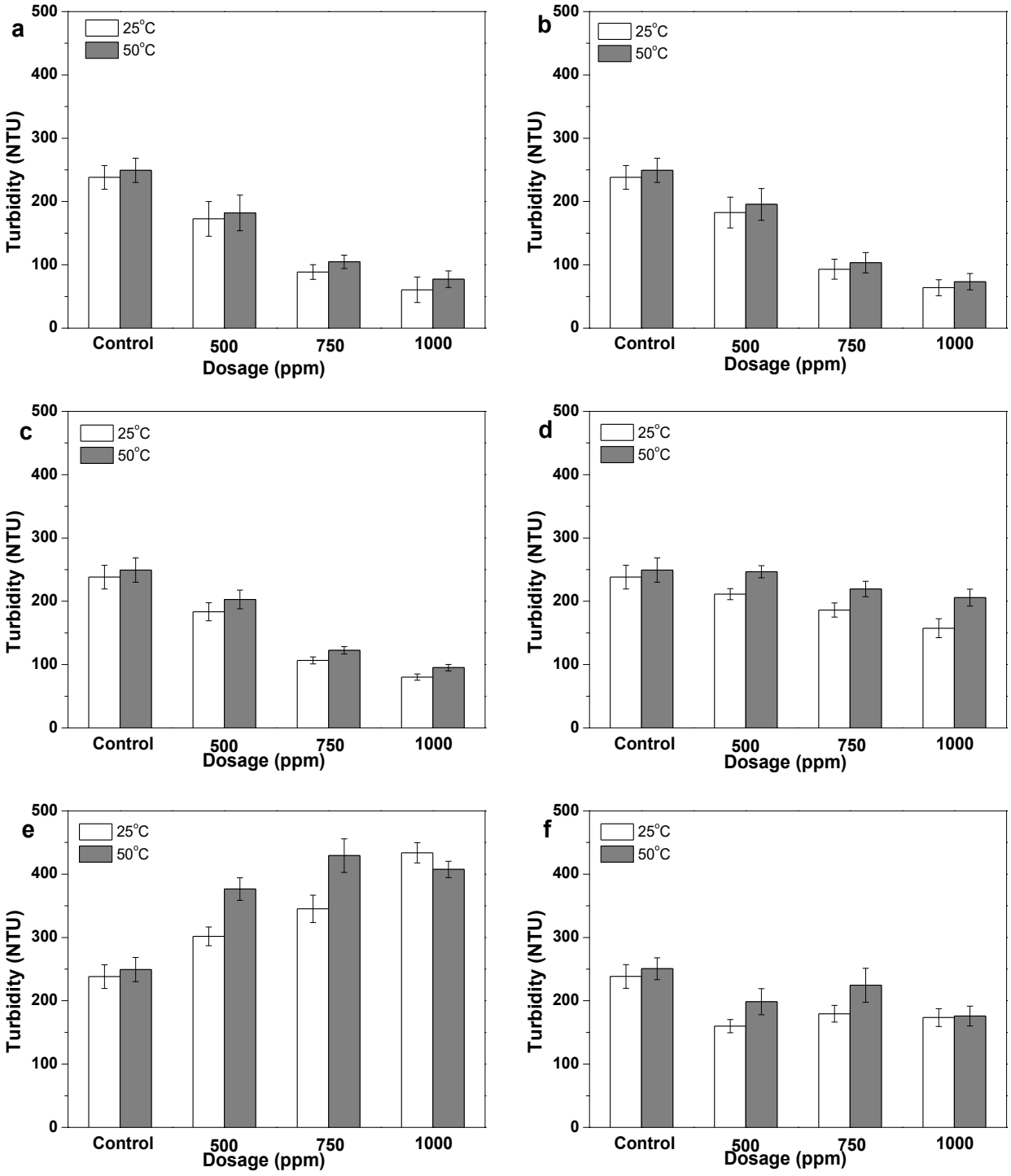

Figure 4.7. Turbidity (NTU) of 10 wt. % MFT treated by:

(a) poly(AAm-*st*-DADMAC) (**D10**), (b) mixture of 70% (wt./wt.) poly(AAm-*st*-DADMAC) (**D7N3**), (c) mixture of 50% (wt./wt.) poly(AAm-*st*-DADMAC) and 50% (wt./wt.) polyNIPAM (**D5N5**), (d) mixture of 30% (wt./wt.) poly(AAm-*st*-DADMAC) and 70% (wt./wt.) polyNIPAM (**D3N7**), (e) polyNIPAM (**N10**), (f) poly(AEMA-*st*-NIPAM).

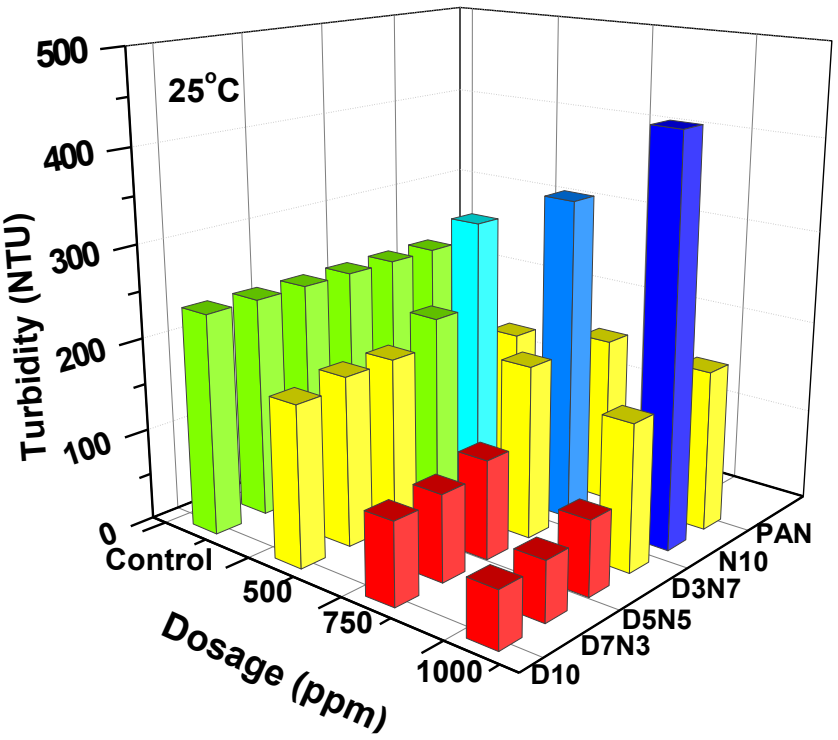

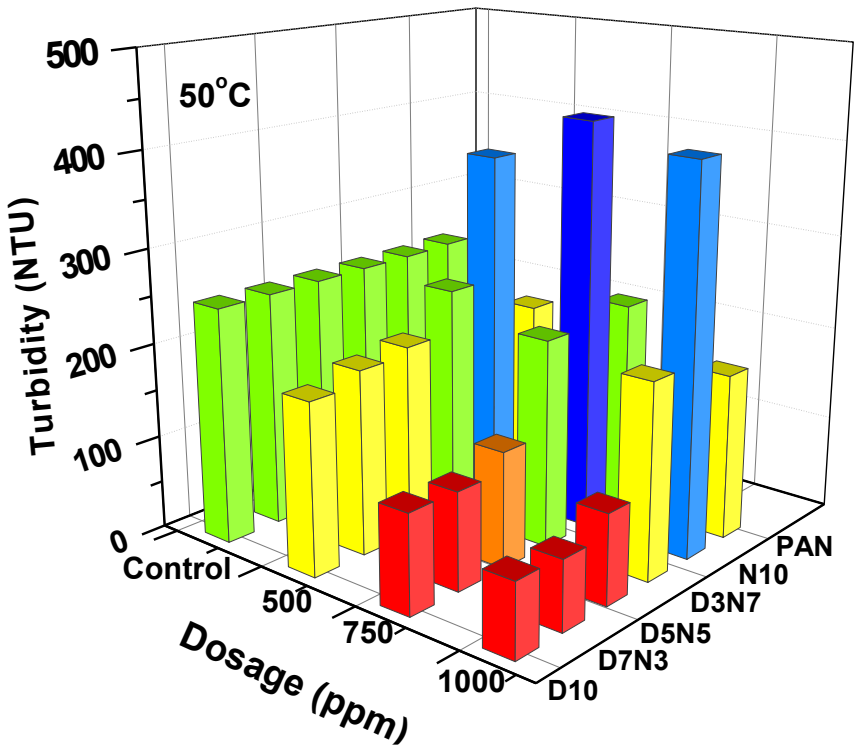

Figure 4. 8 3D graph of turbidity (NTU) of 10 wt. % MFT at 25°C and 50°C.

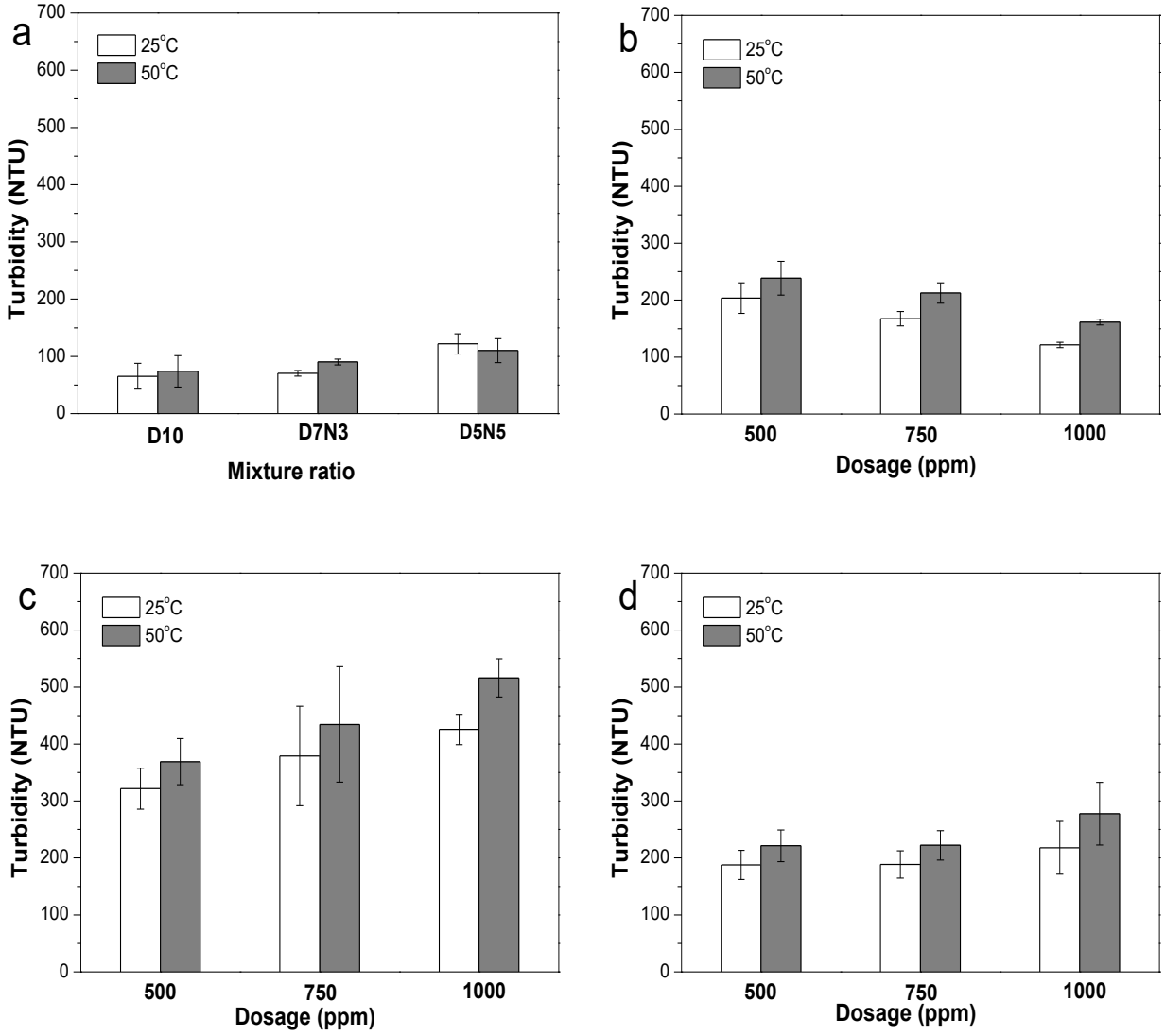

Figure 4.9. Turbidity (NTU) of 15 wt. % MFT treated by:
(a) 1000 ppm of poly(AAm-*st*-DADMAC) (**D10**), mixture of 70% (wt./wt.) poly(AAm-*st*-DADMAC) and 30% (wt./wt.) polyNIPAM (**D7N3**) and mixture of 50% (wt./wt.) poly(AAm-*st*-DADMAC) and 50% (wt./wt.) polyNIPAM (**D5N5**), (b) mixture of 30% (wt./wt.)) poly(AAm-*st*-DADMAC) and 70% (wt./wt.) polyNIPAM (**D3N7**), (c) polyNIPAM (**N10**), (d) poly(AEMA-*st*-NIPAM).

4.3.4 Sediment solids content

The solids content of sediment was determined after 24 hours settling. For the case of 10 wt. %

MFT (Figure 4.10

Figure 4.10. Solids content of 10 wt. % MFT treated by:

(a) poly(AAm-st-DADMAC) (**D10**), (b) mixture of 70% (wt/wt) poly(AAm-st-DADMAC) and 30% (wt./wt.) polyNIPAM (**D7N3**), (c) mixture of 50% (wt./wt.) poly(AAm-st-DADMAC) and 50% (wt./wt.) polyNIPAM (**D5N5**), (d) mixture of 30% (wt/wt) poly(AAm-st-DADMAC) and 70% (wt./wt.) polyNIPAM (**D3N7**), (e) polyNIPAM (**N10**), (f) poly(AEMA-st-NIPAM).

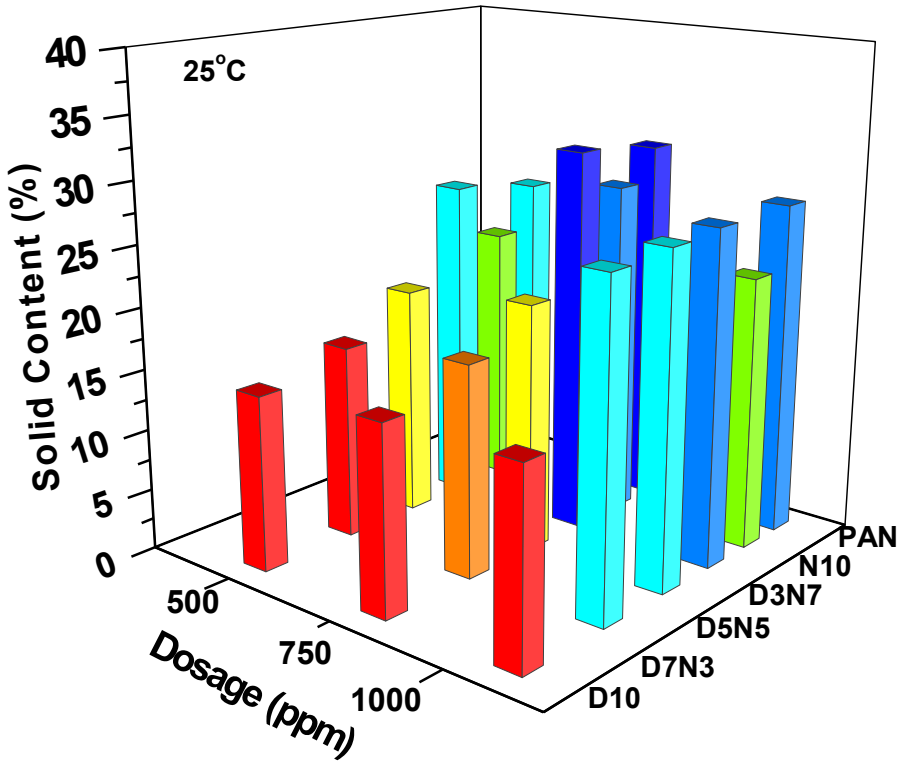

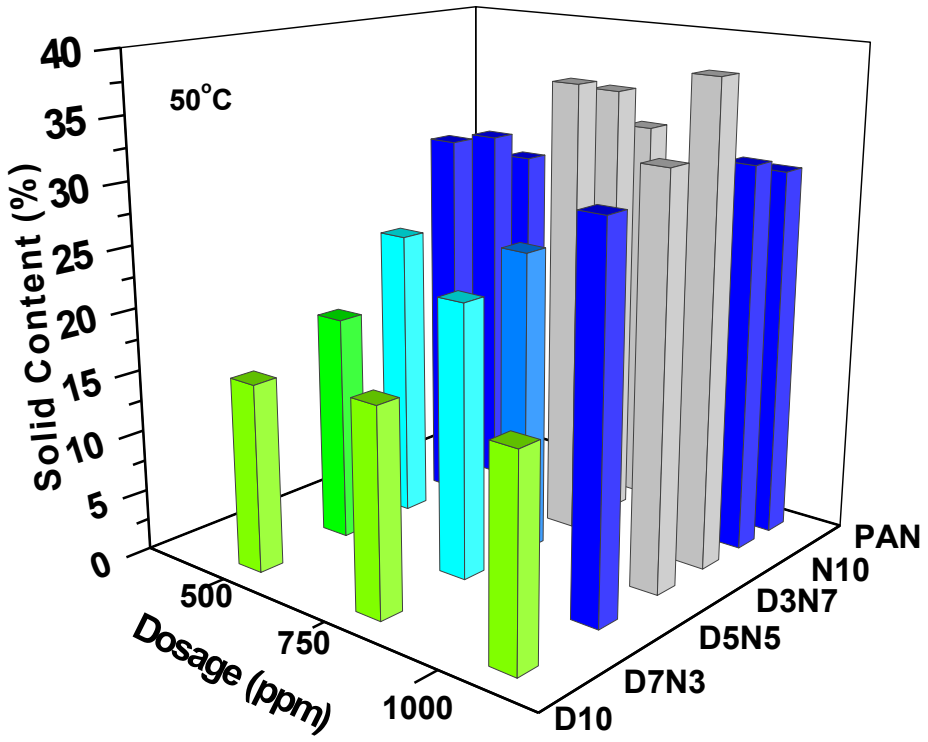

), poly(AAm-*st*-DADMAC) (**D10**) (a) failed to achieve high sediment solids content, and it is not surprising as the sample treated by poly(AAm-*st*-DADMAC) showed highest mudline height (data not shown) and lowest ISR. The results can be explained by the insufficient adsorption of poly(AAm-*st*-DADMAC) thus the particles cannot form big flocs. Increasing the settling temperature from 25 to 50 °C cannot increase the solids content as poly(AAm-*st*-DADMAC) is not temperature-responsive. The solids content results of 10 wt. % MFT suspension treated by D7N3 （Figure 4.10 b) and D5N5 (Figure 4.10 c) were similar, and also higher than the case treated by **D10**, and the solids content increased by adding higher dosage of polymers (from 500 to 1000 ppm) for **D7N3** and **D5N5**. The sediment solids content of the case treated by **D3N7** (Figure 4.10 d) were further enhanced for samples dosed by 500 and 750 ppm, while sample treated by 1000 ppm shows lower solids content compared to 750 ppm (25 °C).The decreased solids

content of sample treated by 1000 ppm may be due to the formation of big flocs, within which water is trapped. But these trapped water can be easily removed from the loose sediment by simple filtration. The secondary enhanced consolidation steps (25 °C →50 °C →25 °C) can also increase the solids content for sample treated by 1000 ppm of **D3N7**. After holding sample at 50 °C for 2 h, then the sample was cooled to 25 °C, and polyNIPAM in the mixture solution would change from hydrophobic to hydrophilic state, and due to the absence of hydrophobic interaction between polymer chains and particles, the flocs collapse into smaller size and fill the gap to further enhance the sediment solids content. The effect of secondary enhanced consolidation is more obvious for sample treated by **N10**. However, the secondary enhanced consolidation steps failed to improve the solids content of sample treated by poly(AEMA-*st*-NIPAM), which can be explained by the electrostatic attraction with particle persists at both 25 °C and 50 °C , and the attraction between particles prevent further consolidation [94]. The summary of solid content results of 10 wt. % MFT is shown in a 3D figure (Figure 4.11). In general, **D5N5** and **D3N7** exhibited higher solid content at 50°C.

The case of 15 wt. % MFT consolidation follows similar trend as 10 wt. % (Figure 4.12). In general, the effect of polymer addition on sediment consolidation is negligible, which might be due to the formation of big flocs and a lots of water is trapped between particles. This results agree with previous reports where Al-PAM was used to enhance sediment consolidation [14]. In order to further improve the sediment solids content, other techniques such as filtration is required. The summary of solid content results of 15 wt. % MFT is shown in a 3D figure (Figure 4.13). In general the polymer addition is not effective to achieve high solid content for 15 wt. % MFT.

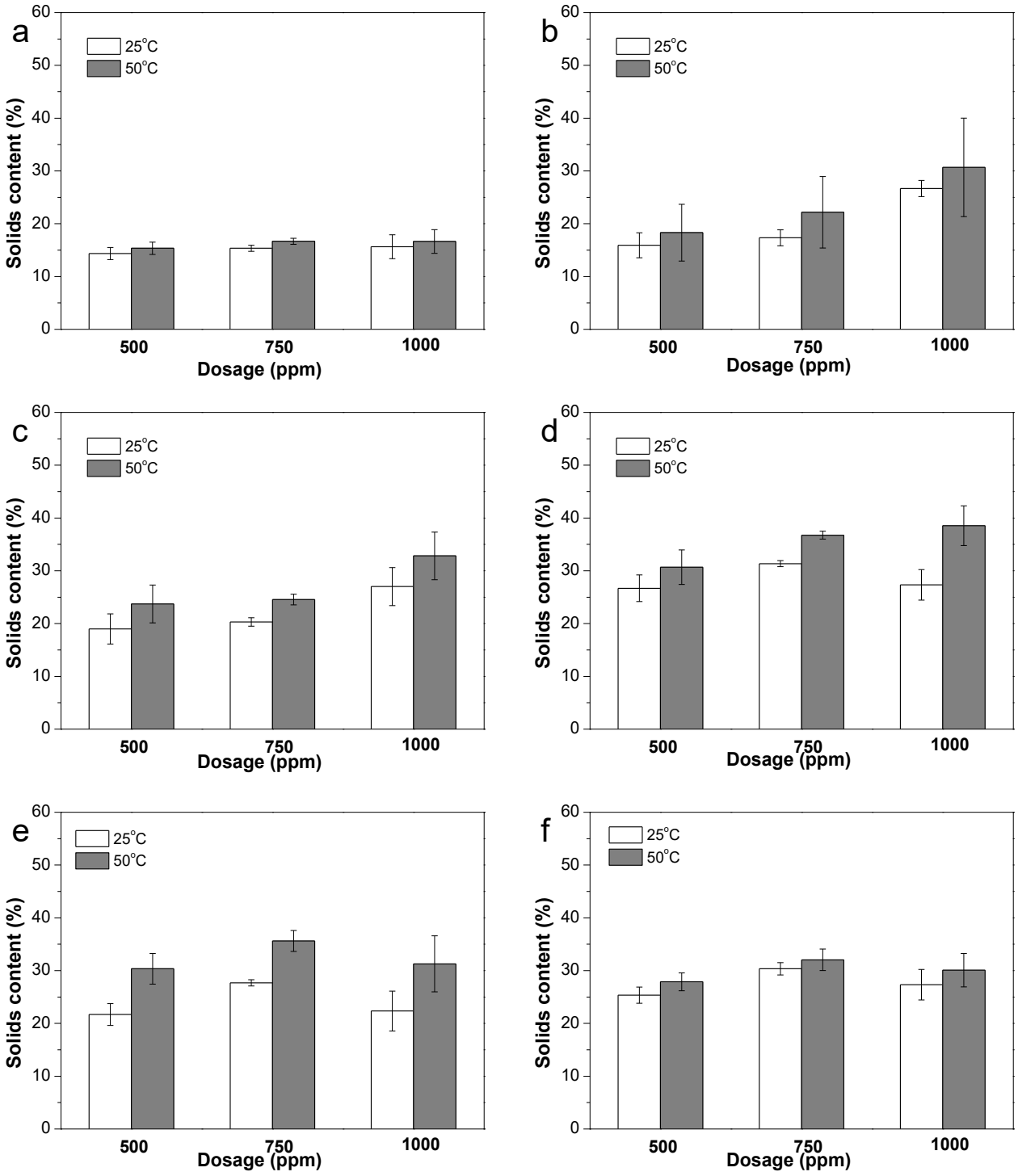

Figure 4.10. Solids content of 10 wt. % MFT treated by:

(b) poly(AAm-*st*-DADMAC) (**D10**), (b) mixture of 70% (wt/wt) poly(AAm-*st*-DADMAC) and 30% (wt./wt.) polyNIPAM (**D7N3**), (c) mixture of 50% (wt./wt.) poly(AAm-*st*-

DADMAC) and 50% (wt./wt.) polyNIPAM (**D5N5**), (d) mixture of 30% (wt/wt) poly(AAm-*st*-DADMAC) and 70% (wt./wt.) polyNIPAM (**D3N7**), (e) polyNIPAM (**N10**), (f) poly(AEMA-*st*-NIPAM).

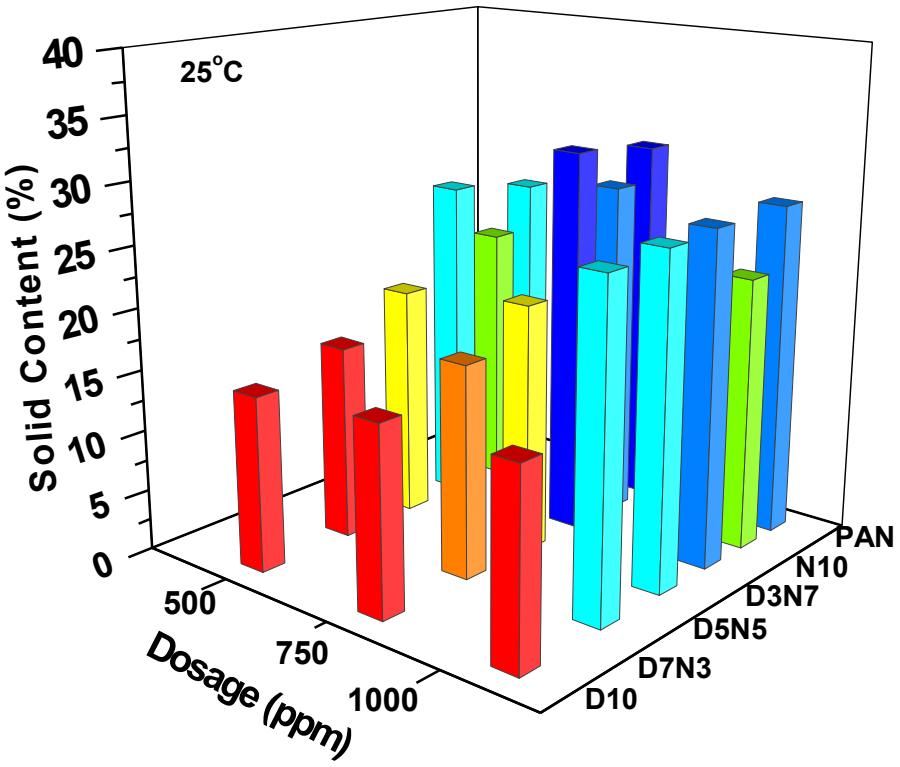

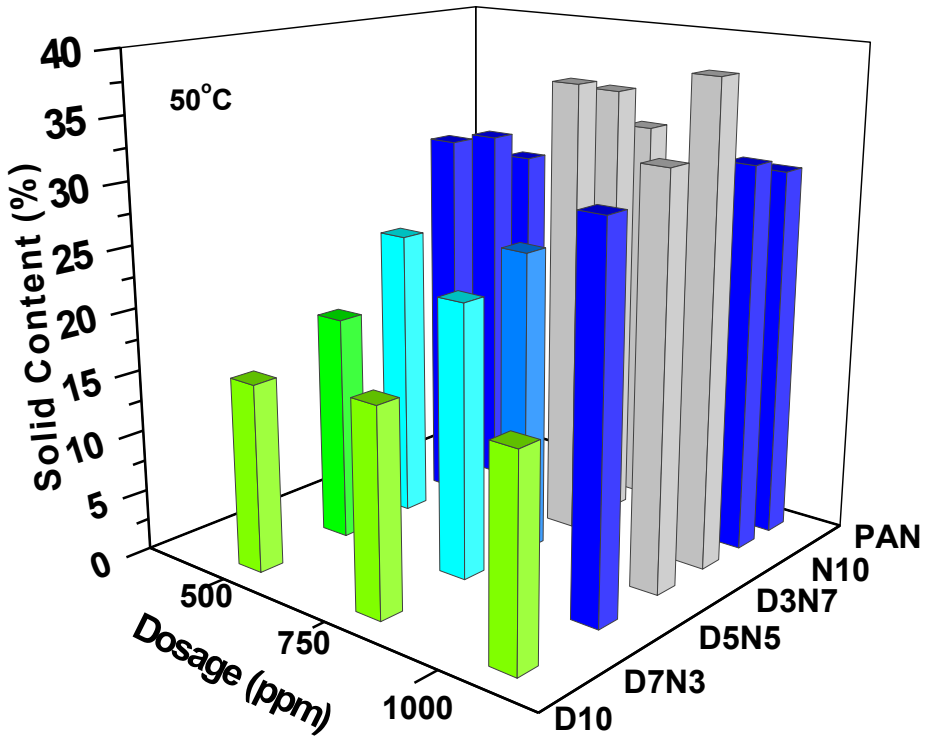

Figure 4.11. 3D graph of solid content (%) of 10 wt. % MFT at 25°C and 50°C.

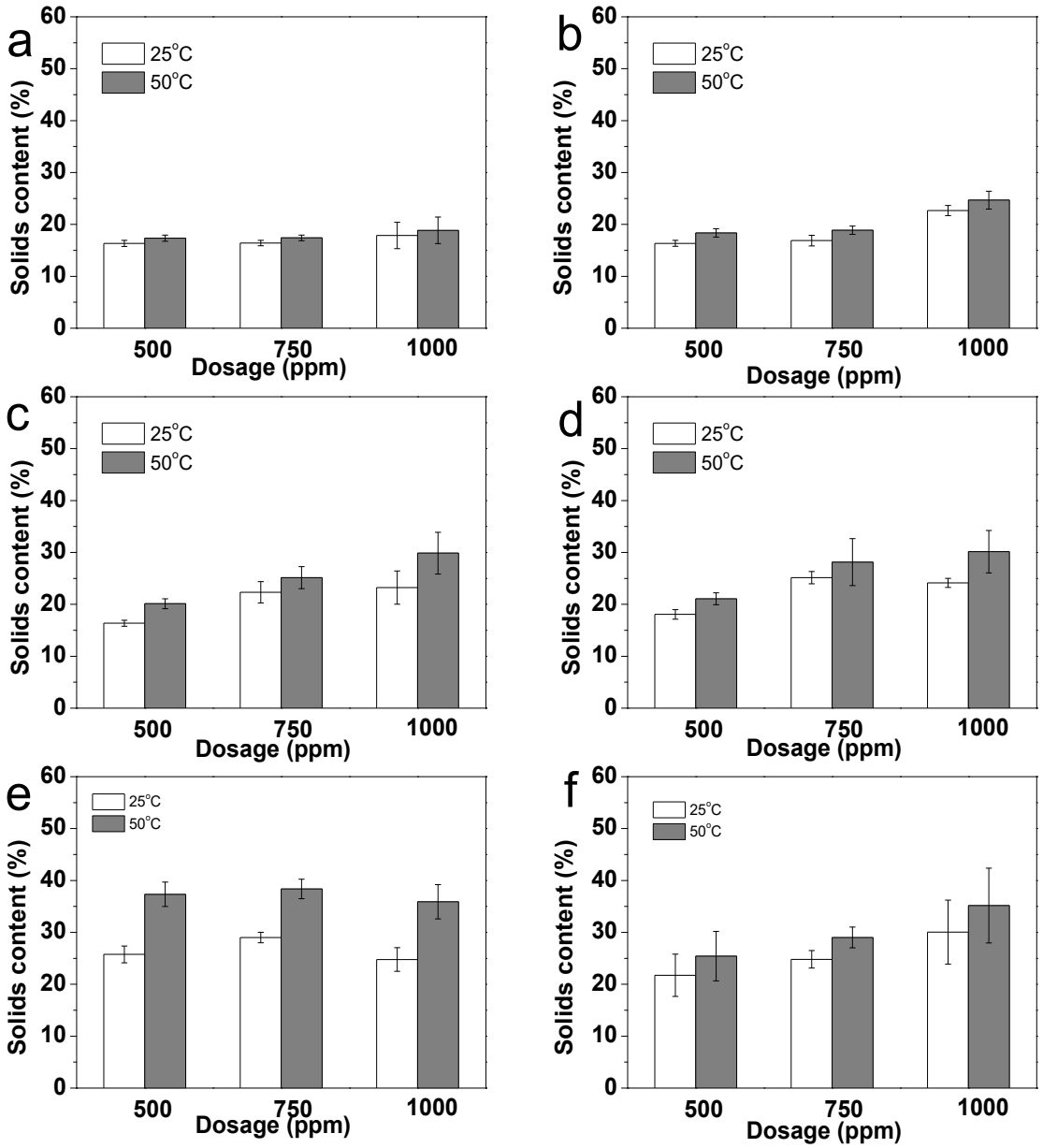

Figure 4.12. Solids content of 15 wt. % MFT treated by:

(a) poly(AAm-*st*-DADMAC) (**D10**), (b) mixture of 70% (wt./wt.) poly(AAm-*st*-DADMAC) and 30% (wt./wt.) polyNIPAM (**D7N3**), (c) mixture of 50% (wt./wt.) poly(AAm-*st*-DADMAC) and 50% (wt./wt.) polyNIPAM (**D5N5**), (d) mixture of 30% (wt./wt.) poly(AAm-*st*-DADMAC) and 70% (wt./wt.) polyNIPAM (**D3N7**), (e) polyNIPAM (**N10**), (f) poly(AEMA-*st*-NIPAM).

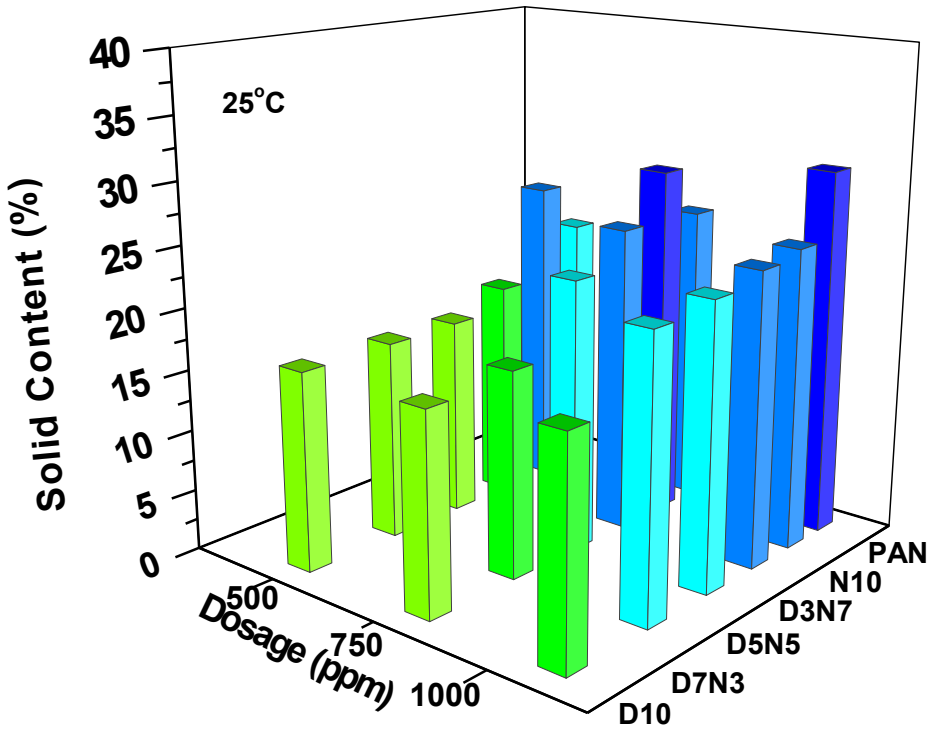
25°C
Solid Content (%)
0
5
10
15
20
25
30
35
40
Dosage (ppm)
500
750
1000
D10
D7N3
D5N5
D3N7
N10
PAN

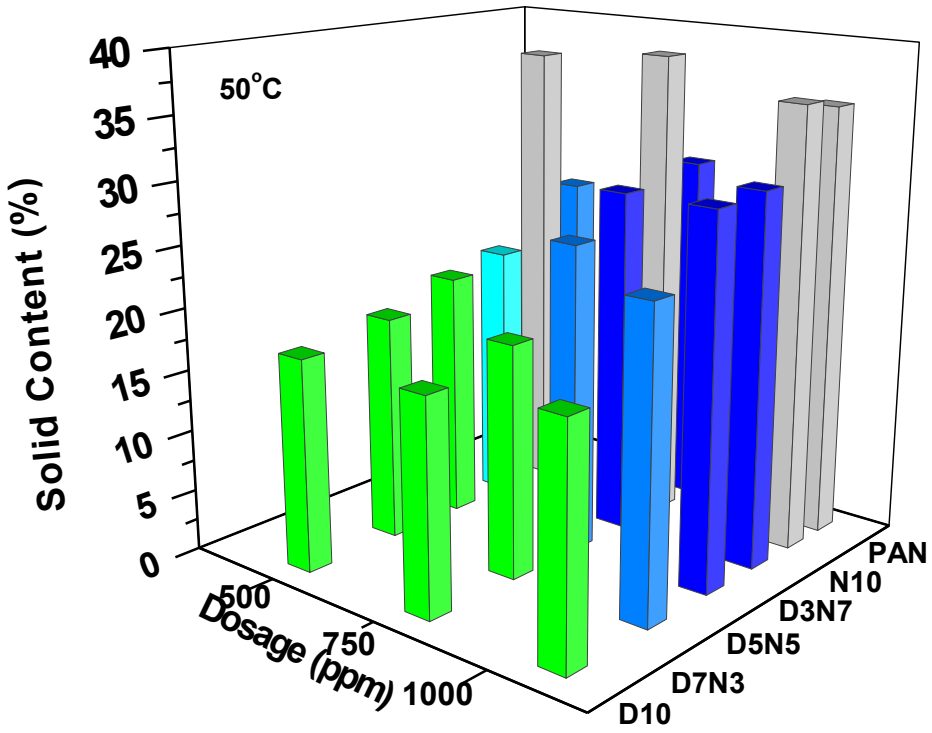

Figure 4.13. 3D graph of solid content (%) of 15 wt. % MFT at 25°C and 50°C.

4.3.5 Water recovery

The water recovery results of 10 wt. % MFT suspension are shown in Figure 4.14. The 10 wt. % MFT suspension treated by **D10** (Figure 4.14 a) exhibits little increment of water recovery compared to the control. After mixing with 30% (wt/wt) polyNIPAM polymer solution the water recovery was significantly increased, especially for the one dosed at 1000 ppm, and the results agree with ISR results, which can be explained by the increased adsorption force of polyNIPAM. 10 wt. % MFT dosed by **D7N3** (Figure 4.14 b) showed similar results to **D5N5** (Figure 4.14 c), and the water recovery increased by adding higher dosage polymer solutions for these two ratios. While for 10 wt. % MFT suspension dosed by **D3N7** (Figure 4.14 d), the increased polymer dosage

from 750 to 1000 ppm can slightly enhance the water recovery, which can further confirm that the decreased solids content of sample treated by 1000 ppm **D3N7** (Figure 4.10 d) is just because water trapped between big flocs, and the loose sediment decreased its solids content, but after filtration the trapped water can easily be recovered. The sample treated by 1000 ppm **N10** (Figure 4.14 e) showed similar phenomenon, and although the solids content of 1000 ppm **N10** was lower than 750 ppm (Figure 4.10 e), the water recovery was almost the same, indicating that water is already removed from MFT particles and is simply trapped between big flocs. While increased polymer dosage of **N10** has little effect on water recovery, which might due to the fact that 500 ppm polyNIPAM is enough to cover the particle surface, and there is not more free space for polymer chain to adsorb. The summary of water recovery results of 10 wt. % MFT is shown in a 3D figure (Figure 4.15). In general, higher water recovery can be achieved when the composition of polyNIPAM higher than 50% (wt. /wt.) (**D5N5**, **D3N7** and **N10**).

The water recovery results of 15 wt. % are shown in Figure 4.16. **D10** (Figure 4.16 a) and **D7N3** (Figure 4.16 b) have not shown significant effect on water recovery. **D5N5** (Figure 4.16 c) and D3N7 (Figure 4.16 d) can achieve higher than 50% water recovery when polymer dosage higher than 750 ppm while 500 ppm of these two ratios cannot even reach 20% of water recovery. 15 wt.% MFT suspension treated by **N10** (Figure 4.16 e) can achieve 50% water recovery at 500 ppm while further addition of polymer could not increase the water recovery due to the limited free spaces on the particle surface for polymer adsorption, which is similar to the results of 10 wt. % MFT. In general, increasing temperature from 25 to 50 °C cannot significantly improve water recovery as for either the case of 10 and 15 wt. % MFT because the sediment bed have already experienced the secondary enhanced consolidation. The summary water recovery results of 15 wt. % MFT is shown in a 3D figure (Figure 4. 17). In order to achieve higher water recovery, higher polymer

dosage is required compared to 10 wt. % MFT.

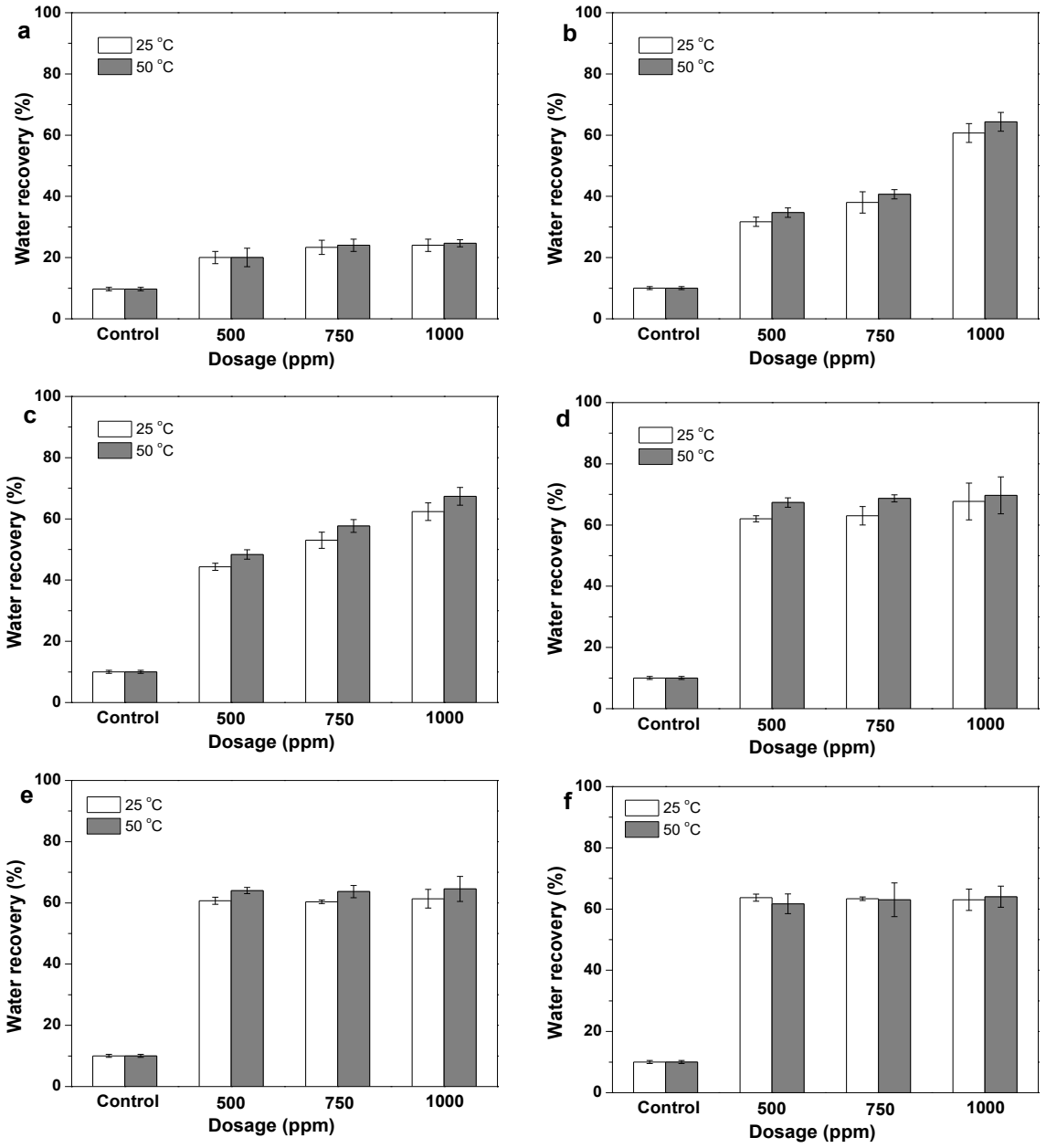

Figure 4.14. Water recovery of 10 wt. % MFT treated by: (a) poly(AAm-*st*-DADMAC) (**D10**), (b) mixture of 70% (wt./wt.) poly(AAm-*st*-DADMAC) and 30% (wt./wt.) polyNIPAM (**D7N3**), (c) mixture of 50% (wt./wt.) poly(AAm-*st*-DADMAC) and 50% (wt./wt.) polyNIPAM (**D5N5**), (d) mixture of 30% (wt./wt.) poly(AAm-*st*-DADMAC) and 70% (wt./wt.) polyNIPAM (**D3N7**), (e) polyNIPAM (**N10**), (f) poly(AEMA-*st*-NIPAM).

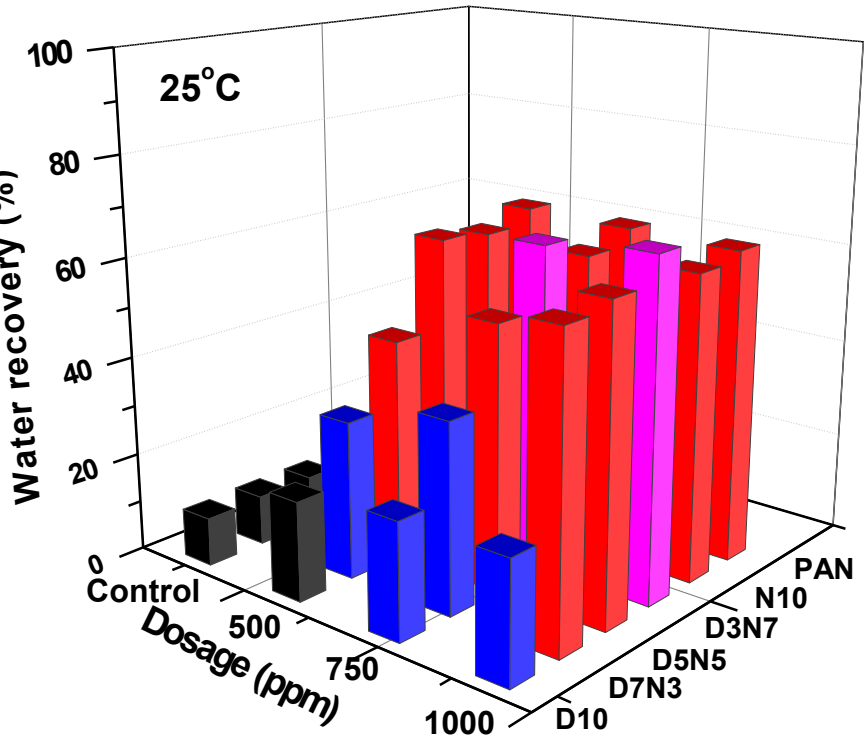
25°C
Water recovery (%)
100
80
60
40
20
0
Control
500
750
1000
Dosage (ppm)
PAN
N10
D3N7
D5N5
D7N3
D10

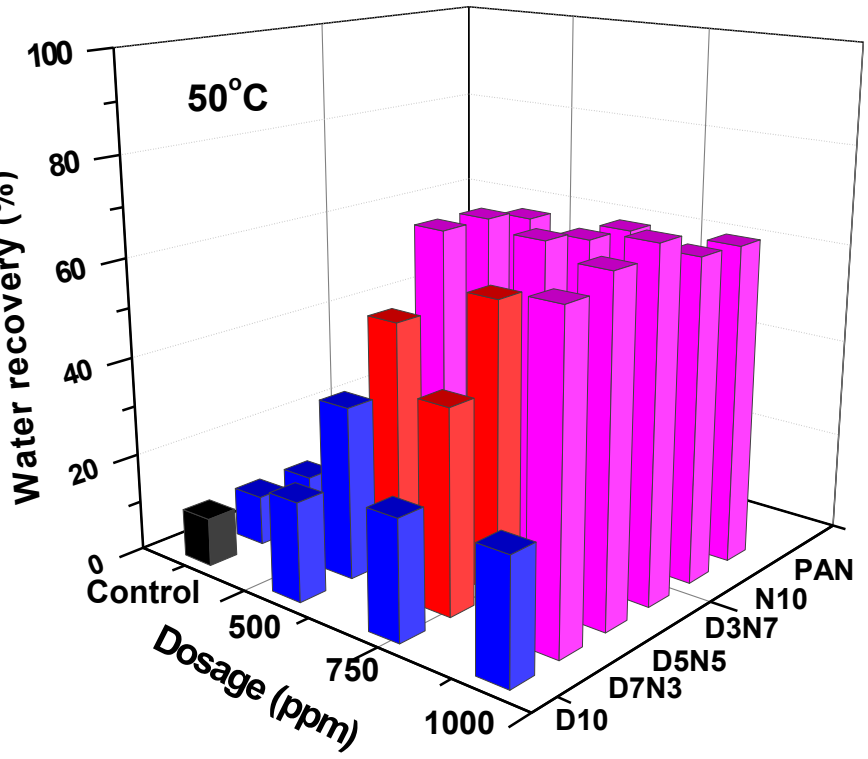

Figure 4.15. 3D graph of water recovery (%) of 10 wt. % MFT at 25°C and 50°C.

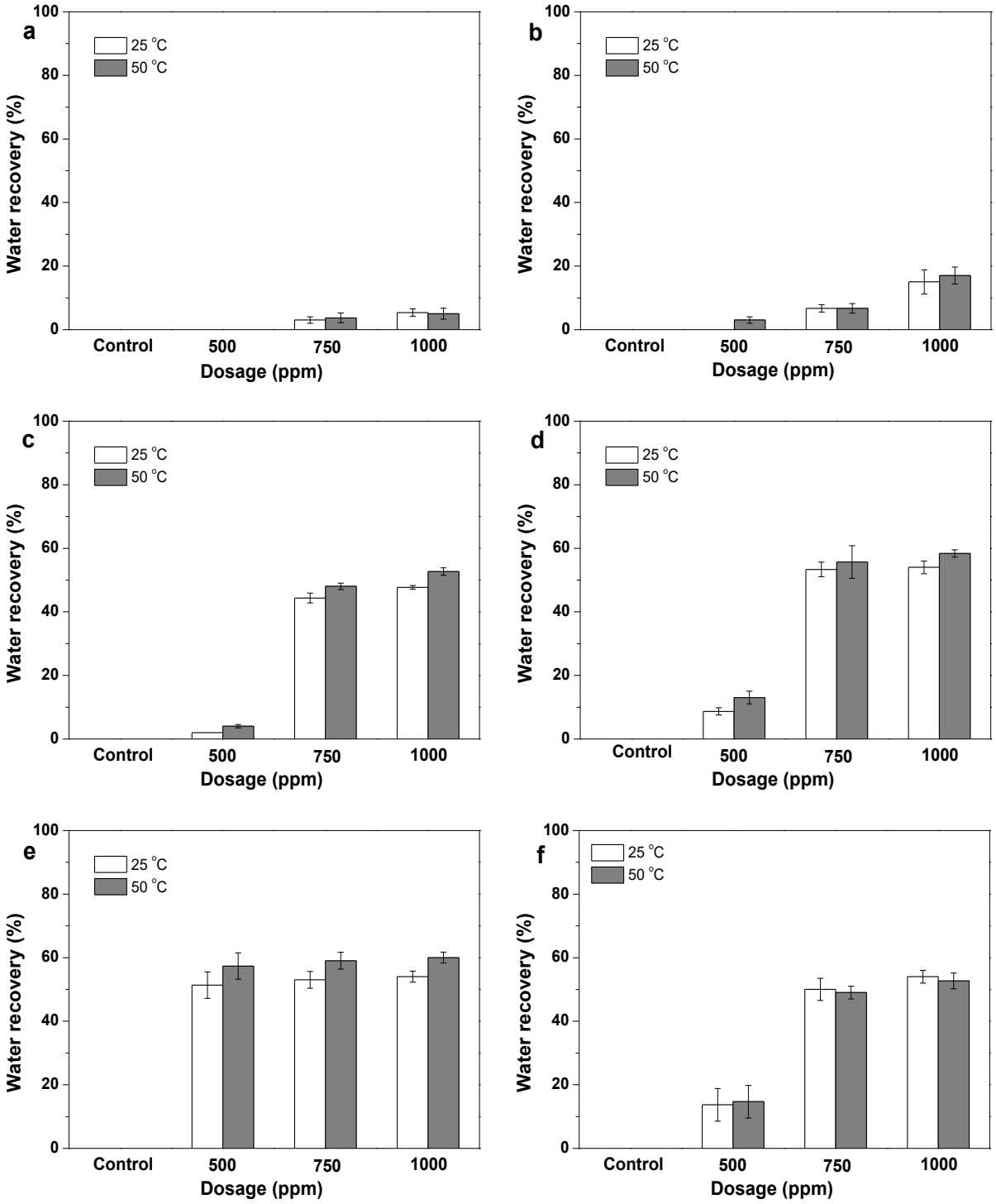

Figure 4.16. Water recovery of 15 wt. % MFT treated by: (a) poly(AAm-*st*-DADMAC) (**D10**), (b) mixture of 70% (wt./wt.) poly(AAm-*st*-DADMAC) and 30% (wt./wt.) polyNIPAM (**D7N3**), (c) mixture of 50% (wt./wt.) poly(AAm-*st*-DADMAC) and 50% (wt./wt.) polyNIPAM (**D5N5**), (d)

mixture of 30% (wt./wt.) poly(AAm-*st*-DADMAC) and 70% (wt./wt.) polyNIPAM (**D3N7**), (e) polyNIPAM (**N10**), (f) poly(AEMA-*st*-NIPAM).

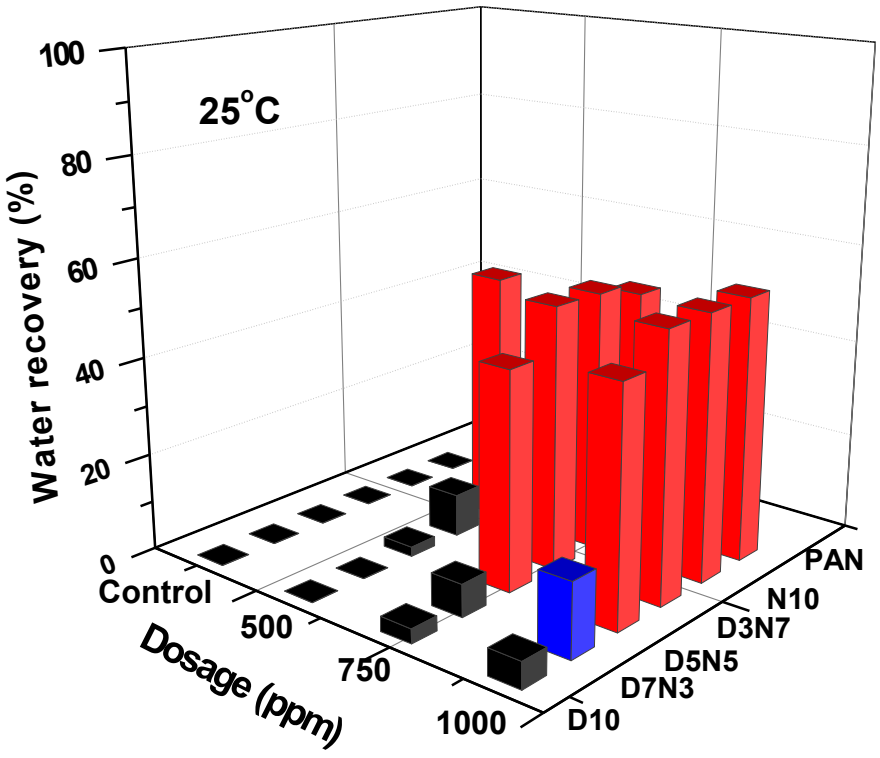

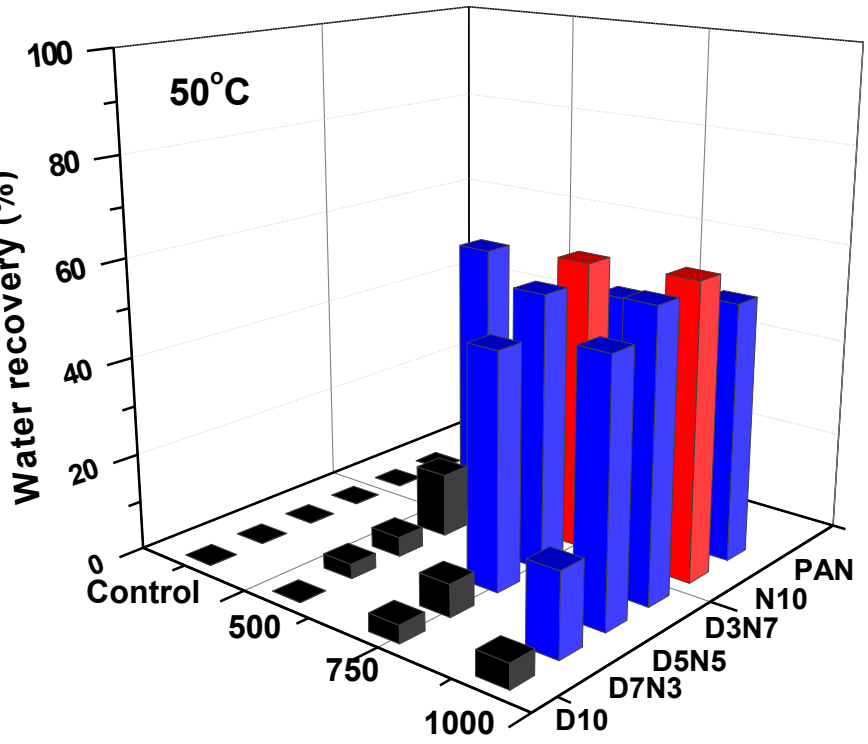

Figure 4. 17 3D graph of water recovery (%) of 15 wt. % MFT at 25°C and 50°C.

4.4 Conclusion

In this study, temperature-responsive polyNIPAM and poly(AEMA-*st*-NIPAM) have been synthesized by conventional free-radical polymerization for solid-liquid separation of MFT suspensions. Neutral polyNIPAM can induce high initial settling rates (ISR) while the supernatant clarity is low. The optimum mixture ratio of polyNIPAM and poly(AAm-*st*-DADMAC) can achieve high ISR and clear supernatant as cationic poly(AAm-*st*-DADMAC) can neutralize the fine negatively charged particles, while poly(AAm-*st*-DADMAC) alone cannot produce high ISR. The secondary enhanced solids content can also be achieved by the mixture of polyNIPAM and poly(AAm-*st*-DADMAC). Moreover, the cationic temperature-responsive poly(AEMA-*st*-

NIPAM) can achieve both high ISR and high clarity at the time because cationic AEMA can neutralize fine charged particles and work as polyelectrolyte to enhance the polymer adsorption onto particles via electrostatic force, while the strong electrostatic interaction between polymer and particles impeded the secondary enhanced consolidation.

Chapter 5 Conclusion and future work

5.1 Major conclusion

The general findings of this thesis research are presented in the following two sections.

5.1.1 Fabrication of antifouling PES/CNC nanocomposite membranes

In this section, PES/CNC nanocomposite membranes were prepared by non-solvent phase-inversion method. The membrane hydrophilicity was determined by contact angle and water content. The PWF, protein rejection and FRR were measured by a dead-end cell system. FRR was used as an indicator of membrane antifouling capacity. SEM was used to investigate the membrane morphology. Membrane pore size was studies by PEG with different molecular weight and the filtered PEG concentration was measured by TOC analyzer. Membrane thermal stability was tested by TGA.

The contact angle and water content results revealed that the hydrophilicity of the membranes enhanced significantly by increasing the CNC content in the casting solution. The pure water flux was improved with an increase of CNC concentration up to 1.0 wt. %, and decreased with further addition of CNC in the casting solution up to 5.0 wt.%. BSA rejection was also improved by increasing CNC content due to the formation of smaller pore size and thicker skin layer of the nanocomposite membranes. The antifouling property was significantly improved after blending CNC as quantified by measuring the flux recovery ratio. Finally, the thermal stability of PES/CNC nanocomposite membrane was found to be lower than unmodified PES membranes.

5.1.2 Flocculation and dewatering of mature fine tailings using temperature-responsive cationic polymers

In this section, temperature-responsive polymers polyNIPAM and poly(AEMA-*st*-NIPAM) were synthesized by conventional free-radical polymerization for investigation of the settling

performance of MFT. The neutral polyNIPAM was mixed with cationic poly(AAm-*st*-DADMAC) and the effect of mixture ratio, temperature and polymer dosage on flocculation of MFT were investigated regarding to four parameters: ISR, supernatant turbidity, solid content and water recovery. GPC and ^{1}H NMR were used to characterize synthesized polyNIPAM and poly(AEMA-*st*-NIPAM). UV-Vis spectrometer was used to measure the clarity of the supernatant and lower critical solution temperature (LCST) of polymers.

In summary, neutral polyNIPAM can induce high initial settling rates (ISR) while the clarity of supernatant is low. The optimum mixture ratio of polyNIPAM and poly(AAm-*st*-DADMAC) can achieve high ISR and clear supernatant as cationic poly(AAm-*st*-DADMAC) can neutralize the fine negative charged particles, while poly(AAm-*st*-DADMAC) alone cannot produce high ISR. The secondary enhanced solids content can also be achieved by the mixture of polyNIPAM and poly(AAm-*st*-DADMAC). Moreover, the cationic temperature-responsive poly(AEMA-*st*-NIPAM) can achieve both high ISR and clarity at the time because cationic AEMA can neutralize fine charged particles and work as polyelectrolyte to enhance the polymer adsorption onto particles via electrostatic force, while the strong electrostatic interaction between polymer and particles impeded the secondary enhanced consolidation of poly(AEMA-*st*-NIPAM).

5.2 Future work

(1) More characterizations of PES/CNC membranes are needed to further understand the membrane properties, such as membrane surface roughness and surface charge.

(2) More research is needed to further study the properties and compositions of MFT produced by different bitumen extraction process, and their effects on the performance of different polymers.

(3) PolyNIPAM synthesized by conventional free-radical polymerization can achieve high ISR,

and cationic poly(AAm-*st*-DADMAC) can achieve high, while the working mechanism of polymers need to be further investigated.

(4) Poly(AEMA-*st*-NIPAM) can achieve both high ISR and low turbidity, while the preparation of AEMA monomer was time-consuming, and the secondary enhanced consolidation of poly(AEMA-*st*-NIPAM) is low due to the strong electrostatic interaction between polymers and particles. Therefore, other methods, such as electrical treatment, can be combined with polyNIPAM to achieve higher ISR, clarity of supernatant and solid content.

References

[1] M. Kummu, P.J. Ward, H. de Moel, O. Varis, Is physical water scarcity a new phenomenon? Global assessment of water shortage over the last two millennia, Environmental Research Letters, 5 (2010) 034006.

[2] A. Demoz, R.J. Mikula, Role of mixing energy in the flocculation of mature fine tailings, Journal of Environmental Engineering, 138 (2011) 129-136.

[3] L.S. Kotlyar, B.D. Sparks, J. Woods, C.E. Capes, R. Schutte, Biwetted ultrafine solids and structure formation in oil sands fine tailings, Fuel, 74 (1995) 1146-1149.

[4] in, Government of Alberta: Environment and Sustainable Resource Department, Environmental Management of Alberta's Oil Sands, 2009.

[5] S. Proskin, D. Sego, M. Alostaz, Freeze–thaw and consolidation tests on Suncor mature fine tailings (MFT), Cold Regions Science and Technology, 63 (2010) 110-120.

[6] X. Li, M. Fung, Creating soil-like materials for plant growth using tailings sand and fine tails, Journal of Canadian Petroleum Technology, 37 (1998).

[7] https://www.ufz.de/index.php?en=37386.

[8] Y. Xu, T. Dabros, J. Kan, Filterability of oil sands tailings, Process Safety and Environmental Protection, 86 (2008) 268-276.

[9] D. Devenny, A screening study of oil sand tailings technologies and practices, Prepared for Alberta Energy Research Institute, (2010).

[10] J. Shang, Electrokinetic sedimentation: a theoretical and experimental study, Canadian Geotechnical Journal, 34 (1997) 305-314.

[11] J.Q. Shang, Electokinetic dewatering of clay slurries as engineered soil covers, Canadian Geotechnical Journal, 34 (1997) 78-86.

[12] J.Q. Shang, A.R. Fernando, E.K. Lam, Electrokinetic dewatering of gypsum containing tailings, in, IN: Tailings and Mine Waste, 2009.

[13] L. Alagha, S. Wang, L. Yan, Z. Xu, J. Masliyah, Probing adsorption of polyacrylamide-based polymers on anisotropic basal planes of kaolinite using quartz crystal microbalance, Langmuir, 29 (2013) 3989-3998.

[14] A. Alamgir, D. Harbottle, J. Masliyah, Z. Xu, Al-PAM assisted filtration system for abatement of mature fine tailings, Chemical engineering science, 80 (2012) 91-99.

[15] Y. Ji, Q. Lu, Q. Liu, H. Zeng, Effect of solution salinity on settling of mineral tailings by polymer flocculants, Colloids and Surfaces A: Physicochemical and Engineering Aspects, 430 (2013) 29-38.

[16] L. Alagha, S. Wang, Z. Xu, J. Masliyah, Adsorption kinetics of a novel organic–inorganic hybrid polymer on silica and alumina studied by quartz crystal microbalance, The Journal of Physical Chemistry C, 115 (2011) 15390-15402.

[17] H. Li, J. Long, Z. Xu, J.H. Masliyah, Flocculation of kaolinite clay suspensions using a temperature‐sensitive polymer, AIChE journal, 53 (2007) 479-488.

[18] H. Lu, Y. Wang, L. Li, Y. Kotsuchibashi, R. Narain, H. Zeng, Temperature-and pH-Responsive Benzoboroxole-Based Polymers for Flocculation and Enhanced Dewatering of Fine Particle Suspensions, ACS applied materials & interfaces, 7 (2015) 27176-27187.

[19] T. Mori, J. Tsubaki, J.-P. O'Shea, G.V. Franks, Hydrostatic pressure measurement for evaluation of particle dispersion and flocculation in slurries containing temperature responsive polymers, Chemical engineering science, 85 (2013) 38-45.

[20] W.S. Ng, R. Sonsie, E. Forbes, G.V. Franks, Flocculation/flotation of hematite fines with anionic temperature-responsive polymer acting as a selective flocculant and collector, Minerals Engineering, 77 (2015) 64-71.

[21] Y. Wang, Y. Kotsuchibashi, Y. Liu, R. Narain, Temperature-responsive hyperbranched amine-based polymers for solid–liquid separation, Langmuir, 30 (2014) 2360-2368.

[22] H. Li, J. Zhou, R. Chow, A. Adegoroye, A.S. Najafi, Enhancing treatment and geotechnical stability of oil sands fine tailings using thermo‐sensitive poly (n‐isopropyl acrylamide), The Canadian Journal of Chemical Engineering, 93 (2015) 1780-1786.

[23] E. Burdukova, N. Ishida, T. Shaddick, G.V. Franks, The size of particle aggregates produced by flocculation with PNIPAM, as a function of temperature, Journal of colloid and interface science, 354 (2011) 82-88.

[24] J.-P. O'Shea, G.G. Qiao, G.V. Franks, Solid–liquid separations with a temperature-responsive polymeric flocculant: effect of temperature and molecular weight on polymer adsorption and deposition, Journal of colloid and interface science, 348 (2010) 9-23.

[25] G.V. Franks, Stimulant sensitive flocculation and consolidation for improved solid/liquid separation, Journal of colloid and interface science, 292 (2005) 598-603.

[26] J.-P. O'Shea, G.G. Qiao, G.V. Franks, Temperature-responsive solid–liquid separations with charged block-copolymers of poly (N-isopropyl acryamide), Langmuir, 28 (2011) 905-913.

[27] S. Sakohara, K. Nishikawa, Compaction of TiO 2 suspension utilizing hydrophilic/hydrophobic transition of cationic thermosensitive polymers, Journal of colloid and interface science, 278 (2004) 304-309.

[28] T. Matsushita, Y. Matsui, N. Shirasaki, Y. Kato, Effect of membrane pore size, coagulation time, and coagulant dose on virus removal by a coagulation-ceramic microfiltration hybrid system, Desalination, 178 (2005) 21-26.

[29] M.U. Siddiqui, A.F.M. Arif, S. Bashmal, Permeability-Selectivity Analysis of Microfiltration and Ultrafiltration Membranes: Effect of Pore Size and Shape Distribution and Membrane Stretching, Membranes, 6 (2016) 40.

[30] K. Praneeth, Synthesis and characterization of novel polymeric membranes for water purification and effluents treatment, in, RMIT University, Australia, 2014.

[31] M. Clever, F. Jordt, R. Knauf, N. Räbiger, M. Rüdebusch, R. Hilker-Scheibel, Process water production from river water by ultrafiltration and reverse osmosis, Desalination, 131 (2000) 325-336.

[32] https://socratic.org/questions/what-is-the-difference-between-osmosis-and-reverse-osmosis, in.

[33] F. Pombo, A. Magrini, A. Szklo, Technology Roadmap for Wastewater Reuse in Petroleum Refineries in Brazil, INTECH Open Access Publisher, 2011.

[34] M.J. Cantow, Polymer fractionation, Elsevier, 2013.

[35] http://www.waters.com/waters/en_GB/GPC---Gel-Permeation-Chromatography-Beginner%27s-Guide/nav.htm?cid=10167568&locale=en_GB.

[36] B.S. Lalia, V. Kochkodan, R. Hashaikeh, N. Hilal, A review on membrane fabrication: Structure, properties and performance relationship, Desalination, 326 (2013) 77-95.

[37] P. Van de Witte, P. Dijkstra, J. Van den Berg, J. Feijen, Phase separation processes in polymer solutions in relation to membrane formation, Journal of Membrane Science, 117 (1996) 1-31.

[38] K.-Y. Chun, S.-H. Jang, H.-S. Kim, Y.-W. Kim, H.-S. Han, Y.-i. Joe, Effects of solvent on the pore formation in asymmetric 6FDA–4, 4′ ODA polyimide membrane: terms of thermodynamics, precipitation kinetics, and physical factors, Journal of Membrane Science, 169 (2000) 197-214.

[39] H. Bokhorst, F. Altena, C. Smolders, Formation of asymmetric cellulose acetate membranes, Desalination, 38 (1981) 349-360.

[40] L. Broens, F. Altena, C. Smolders, D. Koenhen, Asymmetric membrane structures as a result of phase separation phenomena, Desalination, 32 (1980) 33-45.

[41] A.T.A.E.-a. El-gendi, Phase Diagram and Membrane Desalination, in: P.R.Y. Ning (Ed.) Desalination Updates, InTech, 2015.

[42] Z.-X. Low, Q. Liu, E. Shamsaei, X. Zhang, H. Wang, Preparation and characterization of thin-film composite membrane with nanowire-modified support for forward osmosis process, Membranes, 5 (2015) 136-149.

[43] H.H. Horowitz, G. Metzger, A new analysis of thermogravimetric traces, Analytical Chemistry, 35 (1963) 1464-1468.

[44] http://radchem.nevada.edu/classes/chem455/lecture_22__thermal_methods.htm.

[45] K.J. Wiechelman, R.D. Braun, J.D. Fitzpatrick, Investigation of the bicinchoninic acid protein assay: identification of the groups responsible for color formation, Analytical biochemistry, 175 (1988) 231-237.

[46] P.K. Smith, R.I. Krohn, G. Hermanson, A. Mallia, F. Gartner, M. Provenzano, E. Fujimoto, N. Goeke, B. Olson, D. Klenk, Measurement of protein using bicinchoninic acid, Analytical biochemistry, 150 (1985) 76-85.

[47] http://www.shimadzu.com/an/toc/lab/toc-l4.html.

[48] A. Rahimpour, S. Madaeni, Polyethersulfone (PES)/cellulose acetate phthalate (CAP) blend ultrafiltration membranes: preparation, morphology, performance and antifouling properties, Journal of Membrane Science, 305 (2007) 299-312.

[49] J.F. Kim, J.H. Kim, Y.M. Lee, E. Drioli, Thermally induced phase separation and electrospinning methods for emerging membrane applications: A review, AIChE Journal, 62 (2016) 461-490.

[50] A. Rahimpour, S. Madaeni, S. Mehdipour-Ataei, Synthesis of a novel poly (amide-imide)(PAI) and preparation and characterization of PAI blended polyethersulfone (PES) membranes, Journal of membrane science, 311 (2008) 349-359.

[51] K. Khulbe, C. Feng, T. Matsuura, The art of surface modification of synthetic polymeric membranes, Journal of Applied Polymer Science, 115 (2010) 855-895.

[52] B. Van der Bruggen, Chemical modification of polyethersulfone nanofiltration membranes: a review, Journal of Applied Polymer Science, 114 (2009) 630-642.

[53] A. Zularisam, A. Ismail, M. Sakinah, Application and challenges of membrane in surface water treatment, Journal of Applied Sciences, 10 (2010) 380-390.

[54] K.O. Agenson, T. Urase, Change in membrane performance due to organic fouling in nanofiltration (NF)/reverse osmosis (RO) applications, Separation and Purification Technology, 55 (2007) 147-156.

[55] A. Razmjou, J. Mansouri, V. Chen, The effects of mechanical and chemical modification of TiO 2 nanoparticles on the surface chemistry, structure and fouling performance of PES ultrafiltration membranes, Journal of Membrane Science, 378 (2011) 73-84.

[56] J. Pieracci, J.V. Crivello, G. Belfort, Photochemical modification of 10kDa polyethersulfone ultrafiltration membranes for reduction of biofouling, Journal of membrane science, 156 (1999) 223-240.

[57] L.-J. Mu, W.-Z. Zhao, Hydrophilic modification of polyethersulfone porous membranes via a thermal-induced surface crosslinking approach, Applied Surface Science, 255 (2009) 7273-7278.

[58] X. Ma, Y. Su, Q. Sun, Y. Wang, Z. Jiang, Enhancing the antifouling property of polyethersulfone ultrafiltration membranes through surface adsorption-crosslinking of poly (vinyl alcohol), Journal of Membrane Science, 300 (2007) 71-78.

[59] N. Saxena, C. Prabhavathy, S. De, S. DasGupta, Flux enhancement by argon–oxygen plasma treatment of polyethersulfone membranes, Separation and Purification Technology, 70 (2009) 160-165.

[60] D. Rana, T. Matsuura, Surface modifications for antifouling membranes, Chemical reviews, 110 (2010) 2448-2471.

[61] Z. Zhao, Z. Wang, N. Ye, S. Wang, A novel N, O-carboxymethyl amphoteric chitosan/poly (ethersulfone) composite MF membrane and its charged characteristics, Desalination, 144 (2002) 35-39.

[62] M. Sadrzadeh, S. Bhattacharjee, Rational design of phase inversion membranes by tailoring thermodynamics and kinetics of casting solution using polymer additives, Journal of Membrane Science, 441 (2013) 31-44.

[63] M. Amirilargani, M. Sadrzadeh, T. Mohammadi, Synthesis and characterization of polyethersulfone membranes, Journal of polymer research, 17 (2010) 363-377.

[64] B. Khorshidi, J. Hajinasiri, G. Ma, S. Bhattacharjee, M. Sadrzadeh, Thermally resistant and electrically conductive PES/ITO nanocomposite membrane, Journal of Membrane Science, 500 (2016) 151-160.

[65] Y. Zhang, F. Liu, Y. Lu, L. Zhao, L. Song, Investigation of phosphorylated TiO 2–SiO 2 particles/polysulfone composite membrane for wastewater treatment, Desalination, 324 (2013) 118-126.

[66] Y. Zhang, L. Wang, Y. Xu, Effect of doping porous ZrO 2 solid superacid shell/void/TiO 2 core nanoparticles (ZVT) on properties of polyvinylidene fluoride (PVDF) membranes, Desalination, 358 (2015) 84-93.

[67] W. Salim, W.W. Ho, Recent developments on nanostructured polymer-based membranes, Current Opinion in Chemical Engineering, 8 (2015) 76-82.

[68] K.K. Sadasivuni, D. Ponnamma, H.-U. Ko, H.C. Kim, L. Zhai, J. Kim, Flexible NO2 sensors from renewable cellulose nanocrystals/iron oxide composites, Sensors and Actuators B: Chemical, 233 (2016) 633-638.

[69] A. Santamaria-Echart, L. Ugarte, C. García-Astrain, A. Arbelaiz, M.A. Corcuera, A. Eceiza, Cellulose nanocrystals reinforced environmentally-friendly waterborne polyurethane nanocomposites, Carbohydrate Polymers, 151 (2016) 1203-1209.

[70] B. Peng, N. Dhar, H. Liu, K. Tam, Chemistry and applications of nanocrystalline cellulose and its derivatives: a nanotechnology perspective, The Canadian Journal of Chemical Engineering, 89 (2011) 1191-1206.

[71] H. Bai, X. Wang, H. Sun, L. Zhang, Permeability and morphology study of polysulfone composite membrane blended with nanocrystalline cellulose, Desalination and Water Treatment, 53 (2015) 2882-2896.

[72] M. Zaman, H. Liu, H. Xiao, F. Chibante, Y. Ni, Hydrophilic modification of polyester fabric by applying nanocrystalline cellulose containing surface finish, Carbohydrate Polymers, 91 (2013) 560-567.

[73] Y. Baek, J. Kang, P. Theato, J. Yoon, Measuring hydrophilicity of RO membranes by contact angles via sessile drop and captive bubble method: A comparative study, Desalination, 303 (2012) 23-28.

[74] J. Huang, J. Xue, K. Xiang, X. Zhang, C. Cheng, S. Sun, C. Zhao, Surface modification of polyethersulfone membranes by blending triblock copolymers of methoxyl poly (ethylene glycol)–polyurethane–methoxyl poly (ethylene glycol), Colloids and Surfaces B: Biointerfaces, 88 (2011) 315-324.

[75] A. Lorenzen, S.W. Kennedy, A Fluorescence-Based Protein Assay for Use with a Microplate Reader, Analytical Biochemistry, 214 (1993) 346-348.

[76] S.S. Madaeni, Y. Mansourpanah, Chemical cleaning of reverse osmosis membranes fouled by whey, Desalination, 161 (2004) 13-24.

[77] K.J. Howe, M.M. Clark, Fouling of microfiltration and ultrafiltration membranes by natural waters, Environmental science & technology, 36 (2002) 3571-3576.

[78] S. Lentsch, P. Aimar, J.L. Orozco, Separation albumin–PEG: transmission of PEG through ultrafiltration membranes, Biotechnology and bioengineering, 41 (1993) 1039-1047.

[79] P. Qu, H. Tang, Y. Gao, L. Zhang, S. Wang, Polyethersulfone composite membrane blended with cellulose fibrils, BioResources, 5 (2010) 2323-2336.

[80] H.-y. Yu, Z.-y. Qin, Z. Zhe, Cellulose nanocrystals as green fillers to improve crystallization and hydrophilic property of poly (3-hydroxybutyrate-co-3-hydroxyvalerate), Progress in Natural Science: Materials International, 21 (2011) 478-484.

[81] S. Eyley, W. Thielemans, Surface modification of cellulose nanocrystals, Nanoscale, 6 (2014) 7764-7779.

[82] M. Omidvar, M. Soltanieh, S.M. Mousavi, E. Saljoughi, A. Moarefian, H. Saffaran, Preparation of hydrophilic nanofiltration membranes for removal of pharmaceuticals from water, Journal of Environmental Health Science and Engineering, 13 (2015) 1.

[83] M. Omidvar, S. mahmoud Mousavi, M. Soltanieh, A.A. Safekordi, Preparation and characterization of poly (ethersulfone) nanofiltration membranes for amoxicillin removal from contaminated water, Journal of Environmental Health Science and Engineering, 12 (2014) 1.

[84] Y.-q. Wang, T. Wang, Y.-l. Su, F.-b. Peng, H. Wu, Z.-y. Jiang, Protein-adsorption-resistance and permeation property of polyethersulfone and soybean phosphatidylcholine blend ultrafiltration membranes, Journal of membrane science, 270 (2006) 108-114.

[85] T. Hoare, R. Pelton, Engineering glucose swelling responses in poly (N-isopropylacrylamide)-based microgels, Macromolecules, 40 (2007) 670-678.

[86] G. Zhang, Study on conformation change of thermally sensitive linear grafted poly (N-isopropylacrylamide) chains by quartz crystal microbalance, Macromolecules, 37 (2004) 6553-6557.

[87] F. Zhang, C.-C. Wang, Preparation of P (NIPAM-co-AA) microcontainers surface-anchored with magnetic nanoparticles, Langmuir, 25 (2009) 8255-8262.

[88] G. Chen, A.S. Hoffman, Graft copolymers that exhibit temperature-induced phase transitions over a wide range of pH, Nature, 373 (1995) 49-52.

[89] N. Idota, M. Ebara, Y. Kotsuchibashi, R. Narain, T. Aoyagi, Novel temperature-responsive polymer brushes with carbohydrate residues facilitate selective adhesion and collection of hepatocytes, Science and Technology of Advanced Materials, (2016).

[90] H. Li, J. Long, Z. Xu, J. Masliyah, Synergetic role of polymer flocculant in low-temperature bitumen extraction and tailings treatment, Energy & fuels, 19 (2005) 936-943.

[91] C. Wang, D. Harbottle, Q. Liu, Z. Xu, Current state of fine mineral tailings treatment: a critical review on theory and practice, Minerals Engineering, 58 (2014) 113-131.

[92] L.-S. Kang, J.L. Cleasby, Temperature effects on flocculation kinetics using Fe (III) coagulant, Journal of Environmental Engineering, 121 (1995) 893-901.

[93] G. Franks, E. Burdukova, H. Li, N. Ishida, J. O'Shea, MECHANISM RESPONSIBLE FOR FLOCCULATION IN POLY (N-ISOPROPYLACRYLAMIDE) TEMPERATURE RESPONSIVE DEWATERING–ATTRACTIVE INTERACTION FORCES INDUCED BY SURFACE HYDROPHOBICITY, in: 25th International Mineral Processing Congress, Brisbane, Queensland, Australia, 2010, pp. 4057-4067.

[94] J.-P. O'Shea, G.G. Qiao, G.V. Franks, Temperature responsive flocculation and solid–liquid separations with charged random copolymers of poly (N-isopropyl acrylamide), Journal of colloid and interface science, 360 (2011) 61-70.